

# Assimilation of citizen science data in snowpack modeling using a new snow dataset: Community Snow Observations

Ryan L. Crumley<sup>1,2</sup>, David F. Hill<sup>3</sup>, Katreen Wikstrom Jones<sup>4</sup>, Gabriel J. Wolken<sup>4,5</sup>, Anthony A. Arendt<sup>6</sup>, Christina M. Aragon<sup>1</sup>, Christopher Cosgrove<sup>7</sup>, Community Snow Observations Participants<sup>8</sup>

<sup>1</sup>Water Resources Science, Oregon State University, Corvallis, OR 97331, USA

<sup>2</sup>Earth and Environmental Sciences, Los Alamos National Laboratory, Los Alamos, NM 87545, USA

<sup>3</sup>School of Civil and Construction Engineering, Oregon State University, Corvallis, OR 97331, USA

<sup>4</sup>Alaska Division of Geological and Geophysical Surveys, Fairbanks, AK 99709, USA

<sup>5</sup>International Arctic Research Center, University of Alaska Fairbanks, Fairbanks, AK 99775, USA

<sup>6</sup>University of Washington, Applied Physics Laboratory, WA 98105, USA

<sup>7</sup>Geography Department, Oregon State University, Corvallis, OR 97331, USA

<sup>8</sup>Citizen scientists participating in the project Community Snow Observations (CSO)

Correspondence to: Ryan L. Crumley (ryanlcrumley@gmail.com)

## Abstract.

A physically-based snowpack evolution and redistribution model was used to test the effectiveness of assimilating crowd-sourced snow depth measurements collected by citizen scientists. The Community Snow Observations (CSO; [communitysnowobs.org](http://communitysnowobs.org)) project gathers, stores, and distributes measurements of snow depth recorded by recreational users and snow professionals in high mountain environments. These citizen science measurements are valuable since they come from terrain that is relatively under-sampled and can offer *in-situ* snow information in locations where snow information is sparse or non-existent. The present study investigates 1) the improvements to model performance when citizen science measurements are assimilated and 2) the number of measurements necessary to obtain those improvements. Model performance is assessed by comparing time series of observed (snow pillow) and modeled snow water equivalent values, by comparing spatially-distributed maps of observed (remotely sensed) and modeled snow depth, and by comparing fieldwork results from within the study area. The results demonstrate that few citizen science measurements are needed to obtain improvements in model performance and these improvements are found in 62% to 78% of the ensemble simulations, depending on the model year. Model estimations of total water volume from a sub-region of the study area also demonstrate improvements in accuracy after CSO measurements have been assimilated. These results suggest that even modest measurement efforts by citizen scientists have the potential to improve efforts to model snowpack processes in high mountain environments, with implications for water resource management and process-based snow modeling.

## 1 Introduction

The importance of snow in ecosystem function, in both human and natural systems, and in water resource management in western North America cannot be overstated (Bales et al., 2006; Mankin et al., 2015; Viviroli et al., 2007). Internationally, more than a billion people live in watersheds where snow is an integral part of the hydrologic system (Barnett et al., 2005). Snowpack dynamics

- Deleted: 2
- Deleted: 3
- Deleted: 3
- Deleted: 4
- Deleted: 5
- Deleted: 6
- Deleted: 7
- Deleted: 2
- Deleted: 3
- Deleted: 4
- Deleted: 5
- Deleted: 6
- Deleted: 7

Deleted: measurements of

55 in mountainous, headwater catchments play an essential role connecting atmospheric processes and the hydrologic cycle with  
56 downstream water users, agricultural systems, and municipal water systems (Fayad et al., 2017; Holko et al., 2011; Schneider et  
57 al., 2013).

58  
59 Information about snow distribution comes from many sources. First, there are snow datasets in the form of *in-situ* observations  
60 of snowpack conditions, often observations of snow depth or snow water equivalent (SWE). In the United States of America (U.S.),  
61 snow depth and SWE data are collected by the National Resources Conservation Service's (NRCS) Snow Telemetry (SNOTEL)  
62 network using snow pillows and snow courses. Similar national *in-situ* snow observational networks exist in Europe, like the  
63 MeteoSwiss and MeteoFrance programs that include snow depth, snowfall, and SWE datasets. For a comprehensive overview of  
64 snow observations in Europe, including each program name, the location of observations, and agency websites, see the European  
65 Snow Booklet (Haberhorn, 2019). Snow course information is also collected by state programs such as the California Cooperative  
66 Snow Survey in the U.S. and, in the case of Canada, by provincial programs such as the British Columbia Snow Survey. These *in-*  
67 *situ* snow observations provide critical information on snow conditions and snow distribution worldwide, but vast areas of  
68 snowpack remain unsampled.

69  
70 To fill the observational gaps associated with point measurements, we often turn to snow information in the form of remote sensing  
71 (RS) datasets, like the NASA-based Airborne Snow Observatory (Painter et al., 2016) that uses [aerial](#) light detection and ranging  
72 (LiDAR) in catchment-scale study areas. Other catchment-scale snow RS datasets are collected using unmanned aerial systems,  
73 including high-elevation capable drones and balloon-based platforms in conjunction with structure-from-motion photogrammetry  
74 (Bühler et al., 2016; Li et al., 2019). There are also RS datasets covering hemispheric and global scales, like the daily snow-covered  
75 area product from the MODIS satellite or the GlobSnow snow extent product from the European Space Agency (Hall and Riggs,  
76 2016; Luo et al., 2010).

77  
78 Lastly, there are modeled snow datasets, like the Snow Data Assimilation project with a spatial extent that covers large portions of  
79 North America (SNODAS; NOHRSC, 2004). There are physically-based snow models that produce snow information on  
80 catchment- to hemisphere-scales, like iSnowBal, SnowModel, Alpine3D, PBSM, and SNOWPACK, among many others (Marks  
81 et al., 1999; Liston & Elder, 2006a; Lehning et al., 2006; Pomeroy et al., 1993; Lehning et al., 1999). Studies that integrate all of  
82 these types of snow information, *in-situ* observations, RS datasets, and process models, are becoming common in snow research  
83 because they often produce the best results (Sturm, 2015).

84  
85 Assimilation of data into process modeling is a strategy that seeks to incorporate measurements of environmental variables into  
86 the model chain as a 'hybrid' approach to predicting modeled state variables (Carrassi et al., 2018; Kalnay, 2003). There are many  
87 examples of data assimilation in the atmospheric sciences and weather prediction (Rabier, 2005), in weather reanalysis products  
88 (Gelaro et al., 2017; Kalnay et al., 1996; Messinger et al., 2006; Saha et al., 2010), in the hydrological sciences (Han et al., 2012;  
89 McLaughlin, 2002; McMillan et al., 2013; Park and Xu, 2013), and also in snow science (SNODAS; NOHRSC, 2004; Carroll et  
90 al., 2001). Data assimilation schemes in snow science rest on the notion that modeled variables like SWE can be merged with an  
91 *in-situ* observed value at the same location and time using an objective function. This objective, or cost, function quantifies the  
92 differences between the modeled state variable and the observed state (Reichle et al., 2002; Reichle, 2008; McLaughlin, 2002).  
93 These methods can assimilate model state variables, like SWE, using a statistical method like a Kalman filter or they can assimilate

Deleted:

95 model fluxes like snowfall precipitation or snowmelt rates (Carroll et al., 2001; Clark et al., 2006; Magnussen et al., 2014; Reichle,  
96 2008). Other direct insertion assimilation schemes in snow science run the model twice, once without the assimilated data, and a  
97 second time after the *in-situ* observations and correction factors are calculated in order to produce an updated state variable (Liston  
98 and Hiemstra, 2008; Malik et al., 2012; Helmert et al., 2018). Regardless of the method of assimilation, the goal is the same: to  
99 produce a more accurate modeled state variable (snow depth or SWE) in space and time and to reduce uncertainty in the state  
100 variable by using *in-situ* observations to modify the process model output.

102 Snow depth measurements are a type of *in-situ* snowpack observation that can be made accurately and quickly by anyone with a  
103 measuring device. The potential of mobilizing a new type of in-situ snow dataset collected by snow professionals and snow  
104 recreationists is significant because these participants often travel to remote mountainous environments worldwide where in-situ  
105 snow observations are sparse. Consequently, the current study turns to citizen scientists for snow data collection. Citizen science  
106 is a unique tool for research in which scientists request input from the general public on data collection, data analysis, or data  
107 processing (McKinley et al., 2017; Silvertown, 2009; Wiggins and Crowston, 2011). Through citizen science efforts, researchers  
108 access data that are either highly decentralized or concentrated in space, as well as obtain measurements frequently or randomly  
109 in time. The primary advantage is that many people can accomplish data collection at spatial and temporal scales well beyond the  
110 capacity of a single researcher or small group of scientists (Bonney et al., 2009; Cooper et al., 2007; Dickinson et al., 2010). Recent  
111 successful citizen science-based research includes the CrowdHydrology project that monitors stage heights of streams and rivers  
112 (Fienen and Lowry, 2012; Lowry and Fienen, 2013), and the CrowdWater project, which obtains multiple types of crowdsourced  
113 measurements of hydrological variables using a publicly available app (Seibert et al., 2019; van Meerveld et al., 2017). Buytaert  
114 et al. (2014) provides a comprehensive review of the recent challenges and motivations of citizen science in hydrology. This unique  
115 type of data collected by citizen scientists has been used in many natural sciences, and snow hydrology represents a new opportunity  
116 for citizen science-based research.

118 The present study explores the assimilation of a unique type of citizen science-based data in snow modeling: snow depth  
119 measurements collected by citizen scientists traveling in snow covered landscapes worldwide. This new snow dataset and project  
120 is called Community Snow Observations (CSO; [communitysnowobs.org](http://communitysnowobs.org)). The CSO campaign relies on backcountry recreationists  
121 including skiers, snowboarders, snowmachiners, cross country skiers, snowshoers, and snow professionals, including avalanche  
122 forecasters and snow scientists, who visit snowy environments for work and recreation to obtain snow depth measurements of the  
123 snowpack (Hill et al., 2018; Yeeles, 2018). Other citizen science projects are underway in snow science, including research on the  
124 relationship between vernal windows and snow depth (Contosta et al., 2017), snow depth observations using Twitter (King et al.,  
125 2009), and the backyard precipitation measurement campaign called Community Collaborative Rain, Hail, and Snow Network  
126 (Reges et al., 2016). The CSO project adds to a growing body of research accomplished by citizen scientists in the natural sciences,  
127 and demonstrates how CSO measurements can be assimilated into the process model workflow using a simple data assimilation  
128 technique to sometimes improve model results.

130 The current study aims to answer two questions. First, can citizen scientists' snow depth measurements be incorporated into the  
131 process model workflow in a way that improves model performance? This question is addressed by presenting an ensemble of  
132 modeled snow depth and SWE distribution results with two types of outputs: (a) a set of model outputs without any snow depth  
133 measurements assimilated and, (b) a set of model outputs with CSO snow depth measurements assimilated. To answer this first

Deleted: type of

Deleted: gather

Deleted: The CSO project adds to a growing body of research accomplished by citizen scientists in the natural sciences, and demonstrates how CSO measurements can be assimilated into the process model workflow using SnowAssim to sometimes improve model results

141 question, we characterize the results using temporal and spatial datasets for validation. These datasets include time-series SWE  
 142 observations at a SNOTEL station in the study area and LiDAR- and photogrammetry-derived snow depth maps from 2017 and  
 143 2018. We rely upon common metrics for characterizing the spatial distribution of modeled versus observed continuous  
 144 environmental variables to assess the value of the CSO modified outputs (Riemann et al., 2010). Secondly, how do the results vary  
 145 with the number of the CSO measurements assimilated? We address this question by randomly selecting and varying the quantity  
 146 of CSO measurements in the ensemble members.

148 **2 Study Area**

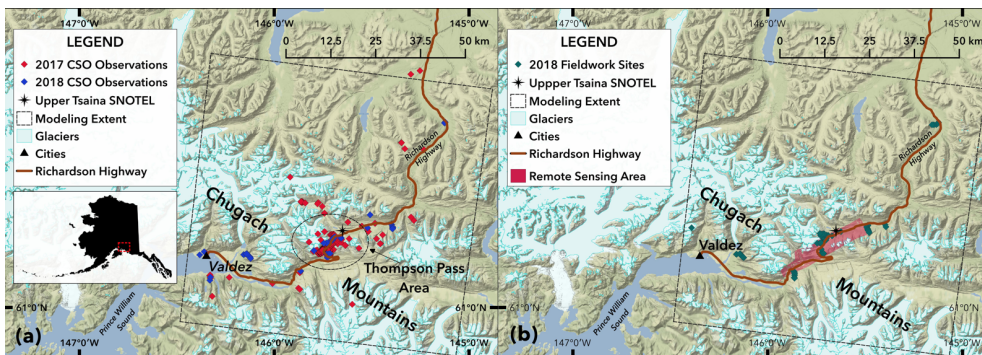
149 The study focuses on a 5,736 km<sup>2</sup> area of the eastern Chugach Mountains near Valdez, Alaska, USA (Figure 1a). This high-relief,  
 150 glacier-carved landscape ranges from sea-level in Port Valdez to rugged peaks exceeding 2200 m.a.s.l., and a mountain pass on  
 151 the Richardson Highway, named Thompson Pass (815 m.a.s.l.). This region of the Chugach Mountains receives extreme amounts  
 152 of snowfall, with Thompson Pass holding multiple snowfall records for the state of Alaska, including the 1-day total (1.57 m), 2-  
 153 day total (3.06 m), and weekly total (4.75 m; Shulski and Wendler, 2007). Like other places in the Chugach Mountains, snow  
 154 densities and snow depths in the region vary greatly across short distances (Wagner, 2012). There are deep, dense, and wet  
 155 snowpacks found in the maritime coastal zone. The interior regions of the Chugach Mountains further from the coast contain  
 156 shallower, less-dense, and drier snow climates (Sturm et al., 1995; Sturm et al., 2010a). These factors are important because the  
 157 Thompson Pass region and the Chugach mountains are frequently accessed by backcountry skiers and snowboarders, backcountry  
 158 snowmachiners, and multiple heli-skiing operations due to the exceptional access to steep terrain, and deep, mountain snowpack  
 159 (Carter et al., 2006; Hendrikx et al., 2016). Due to the popularity of the area for backcountry snowsports and the risk of danger for  
 160 avalanches affecting highway conditions, the Valdez Avalanche Center produces avalanche forecasts for many of the slopes  
 161 adjacent to the Richardson Highway in the Thompson Pass region. The choice of a study area within a mountainous region visited  
 162 regularly by snow recreationists and professionals is essential for the present study. For these reasons, the Thompson Pass region  
 163 of the Chugach Mountains in Alaska was selected for the initial phases of the CSO project.

Deleted: The potential of mobilizing a new type of *in-situ* snow dataset collected by snow professionals and snow recreationists is significant because these participants often travel to remote mountainous environments worldwide where *in-situ* snow observations are sparse.

Deleted: m

Deleted: snow climates near the coast

164



165

166 **Figure 1: Study Area Map and Fieldwork Sites.**  
 167 (a) The study area maps showing the Community Snow Observations (CSO) measurements, the modeling spatial extent, and the  
 168 Thompson Pass region of the Chugach Mountains. (b) The 2018 fieldwork includes 72 sites with co-located snow water equivalent and

Moved (insertion) [1]

176  
177

snow depth measurements. The remote sensing datasets from 2017 and 2018 are overlain on the map, along with the location of the Upper Tsaina SNOTEL station.

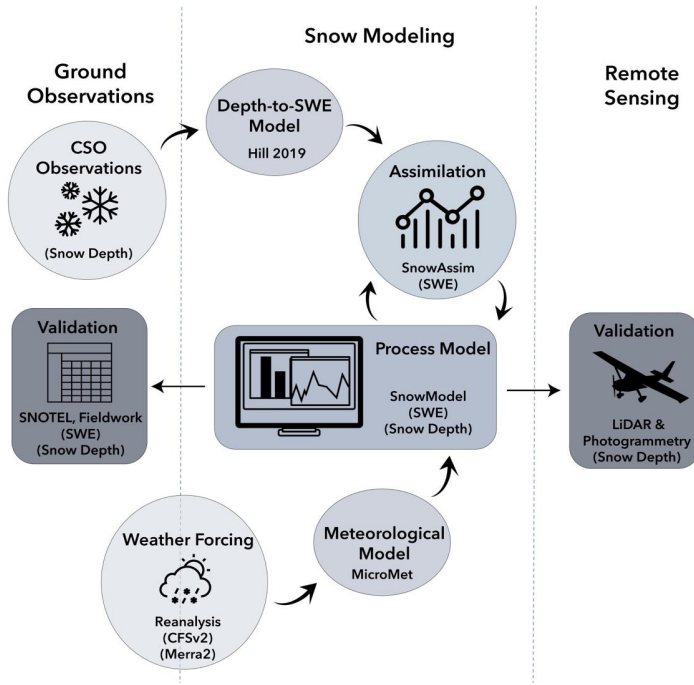
Deleted: and Sugarloaf SNOTEL stations  
Deleted:

178 **3 Methods and Datasets**

179 **3.1 Model Dataflow**

180 This study relies on a common research design in snow science that uses (1) *in-situ* snow observations, (2) physically-based process modeling, and (3) remote sensing of the snowpack to accomplish its primary objectives (Sturm, 2015). Figure 2 is a conceptual diagram of how the citizen scientists' snow depth measurements fit into the model chain for the present study. The modeling process begins with the weather forcing products and citizen scientists' snow depth observations as model inputs. Sub-models for meteorological variable distribution, snow depth to SWE estimation, and for the assimilation of snow measurements are employed before the final simulation occurs. The process model outputs are then validated by the RS datasets, the SNOTEL station record, and the 2018 field measurements. Incorporating the citizen scientists' observations into the model chain is an attempt to modify the model outputs by *in-situ* snow depth observations.

188



189

190

191

192

193

194

Figure 2: Model Dataflow Diagram.

The model chain begins with the weather forcing product and the Community Snow Observations (CSO) datasets. The arrows indicate dataflow through the series of sub-models to the process model output. The model output is then validated by the SNOTEL station time-series, the 2018 fieldwork, and the remote sensing datasets.

197 **3.2 Modeling Framework**

198 In this study we used a sequence of models to simulate SWE and snow depth distributions within the Thompson Pass study area  
199 during WY2017 and WY2018. The sections below provide brief information about the models used in this study. For more details,  
200 please refer to the source citations for each model.  
201

202 **3.2.1 SnowModel**

203 SnowModel (Liston & Elder, 2006a) is a physically-based, spatially distributed process model for simulating the evolution of  
204 snowpacks in snowy environments, and has been used for high-resolution and hemispheric-scale modeling worldwide (Beamer et  
205 al., 2016; Beamer et al., 2017; Crumley et al., 2019; Liston and Hiemstra, 2011; Mernild et al., 2017a-b). We chose SnowModel  
206 for the Chugach Mountains study area because it contains a data assimilation sub-model, SnowAssim, and a snow transportation  
207 sub-model, SnowTran3d. Within SnowModel, various other sub-models solve the energy budget for the snowpack, generate runoff  
208 quantities, etc. The present study focuses on the snow depth and SWE distribution outputs from SnowModel from simulations with  
209 and without the data assimilation sub-model.  
210

Deleted: is chosen

Deleted: since

211 **3.2.2 MicroMet**

212 MicroMet (Liston & Elder, 2006b) is a meteorological distribution sub-model for weather station or reanalysis datasets that can be  
213 paired with SnowModel in spatially explicit modeling applications. MicroMet uses the Barnes objective analysis scheme for  
214 interpolating meteorological input variables to the gridded SnowModel domain for each model timestep (Barnes, 1964; Barnes,  
215 1973). In the present study, instead of using local weather station data, the model is forced with reanalysis data and MicroMet uses  
216 the node locations as weather stations, accessing the reanalysis node surface level precipitation, wind speed and wind direction,  
217 relative humidity, air temperature, and elevation variables for the spatial interpolation. MicroMet has been paired with reanalysis  
218 weather products and SnowModel in many studies worldwide (Baba et al., 2018; Beamer et al., 2016; Liston & Hiemstra, 2011;  
219 Mernild et al., 2017a).  
220

221 **3.2.3 SnowTran3d**

222 Wind redistribution of snow is an important factor for the spatial distribution of snow depths and SWE distributions for snow  
223 modeling (Clark et al., 2011). Wind events build snow deposits in the gullies and the leeward side of bedrock features into drift  
224 depths greater than 10 m at times within the Thompson Pass study area. These events also leave some portions of the landscape  
225 completely scoured and void of snow based on fieldwork observations and the RS snow surveys from both years. SnowTran3d is  
226 a sub-model within SnowModel that redistributes the snow laterally in the model grid according to the processes that govern snow  
227 transportation: fetch, wind speed, wind direction, wind shear stress and the shear strength of the snowpack, saltation and turbulent  
228 suspension of the snow, and sublimation (Liston et al., 2007). SnowTran3d is suitable for use as a sub-routine within SnowModel  
229 when the model grid cell resolution is appropriate for the length scale of snow transportation processes to occur, for example,  
230 primarily at model resolutions less than 100 m.  
231

234 **3.2.4 SnowAssim**

235 To assimilate the CSO measurements, we used the sub-model SnowAssim developed in tandem with SnowModel (Liston and  
236 Hiemstra, 2008). The SnowAssim data assimilation scheme is relatively simple when compared to other assimilation methods.  
237 Direct insertion methods often insert the observed state values into the modeled field in the locations and times where data is  
238 available (McGuire et al., 2006; Fletcher et al., 2012). Hedrick et al. (2018) outlines a ‘modified’ direct insertion method, where  
239 Airborne Snow Observatory LiDAR-based snow depth distributions are input into the iSnobal workflow to modify model state  
240 variables before a new initialization of the model begins. Liston and Hiemstra (2008) describe a different type of modified direct  
241 insertion assimilation scheme (SnowAssim) used in the present study. SnowAssim requires the model to be run twice and pauses  
242 at the end of the first model run. During this pause, differences between the observed SWE depths and modeled SWE depths in  
243 time and location are calculated and interpolated to the entire model domain in the form of a correction surface. The final correction  
244 surface is spatially distributed (for each day of observations) using the Barnes interpolation scheme. These correction surfaces are  
245 then applied to the precipitation inputs and snowmelt factors during the second model run.

246 Note that CSO measurements are submitted as snow depth (m), but the SnowAssim model code and physical equations require  
247 observational inputs to be SWE depth (m), so a conversion from depth to SWE was necessary. The snow depth to SWE conversion  
248 method for the current study will be discussed in the following section. The model determines the dominant snow season phase  
249 (accumulation or ablation), and applies the correction factor surface to either a) the precipitation fluxes or b) the snowmelt factors  
250 during the second model simulation. Additionally, the Barnes interpolation scheme determines outliers within the observed dataset  
251 and determines the degree to which the assimilated values fit the modeled values. This determination creates a smoothed  
252 representation of the observed dataset in the assimilation results. For extensive details about the data assimilation scheme, see  
253 Liston and Hiemstra (2008), their section 3, 4, and 5.

254 Other data assimilation methods include particle-batch smoother and particle filters. These are Bayesian data assimilation methods  
255 used to estimate system state variables based on predicted estimates (modeled) and noisy measurement data (observed). These  
256 types of data assimilation methods rely heavily on characterizing and incorporating the predicted estimate uncertainties and  
257 measurement uncertainties into the analysis using probability distribution functions (Magnusson et al. 2017; Margulis et al. 2015).  
258 In direct insertion or modified direct insertion methods like SnowAssim, modeled and observed state variable uncertainties are not  
259 explicitly characterized.  
260  
261  
262

263 **3.2.5 Snow Depth to Snow Water Equivalent Conversion**

264 CSO participants take measurements of snow depth yet SnowAssim requires SWE observation inputs. A conversion from snow  
265 depth to SWE was necessary for the present study. A body of research exists on the best methods for converting point measurements  
266 from snow depth to SWE, using either bulk density estimations, snow climate classifications, statistical models, or atmospheric  
267 conditions and energy balance approaches (Sturm et al., 1995; Sturm et al., 2010a; McCreight et al., 2014; Jonas et al., 2009;  
268 Pagano et al., 2009; Hill et al., 2019; Pistocchi, 2016). The Hill et al. (2019) model was chosen for two reasons. First, the data  
269 requirements are minimal for this model, requiring only location, day of water year (DOY) and readily-available climatological  
270 information based on input location. These minimal requirements align with the information available from CSO measurements.

Deleted: in order

Formatted: Font: Not Bold

Deleted: Differences between the observed SWE depths and modeled SWE depths in time and location are calculated and interpolated to the entire model domain in the form of a correction surface. The final correction surface is spatially distributed (for each day of observations) using the Barnes interpolation scheme.

Deleted: Note that CSO measurements are submitted as snow depth (m) and SnowAssim requires observational inputs to be SWE depth (m), so a conversion from depth to SWE was necessary

Deleted: Next, t

Deleted: ,

Deleted: a

Deleted:

Deleted: methods

Deleted: using

288 Second, it was found to outperform other bulk density methods such as Sturm et al. (2010) and Jonas et al. (2009) when tested  
289 against a wide variety of snow pillow and snow course datasets, with an overall bias of 0.2 cm and RMSE in SWE of 6 cm (Hill  
290 et al., 2019).

Deleted: m

### 292 3.3 Model Input Datasets

#### 293 3.3.1 Elevation and Land Cover

294 SnowModel requires a digital elevation model (DEM) and a land cover model as two of the three primary input datasets. The DEM  
295 is the National Elevation Dataset (NED) from the United States Geological Survey downloaded at 30 m resolution and then rescaled  
296 to 100 m spatial resolution (Gesch et al., 2009). The land cover model is the National Land Cover Database (NLCD) 2011 dataset  
297 at 30 m spatial resolution and then resampled to 100 m resolution (Homer et al., 2015). The NLCD dataset was reclassified to  
298 match the land cover input classes required by SnowModel. Initially, we tested results from model simulations at two spatial  
299 resolutions, 30 m and 100 m, covering the Thompson Pass model domain. After calibrating the model, the results section only  
300 includes the 30m resolution.

Deleted: in the Thompson Pass region of the Chugach mountains...

#### 302 3.3.2 Weather Forcing Datasets

303 Various weather reanalysis products have been used in remote portions of Alaska in previous studies (Beamer et al., 2016; Beamer  
304 et al., 2017; Crumley et al., 2019; Liston and Hiemstra, 2011). In Alaska, each reanalysis product shows bias corresponding to  
305 meteorological variable, regional location, and season of the year (Lader et al., 2016; see their Figures 3 and 4). For this reason,  
306 the current study considered two weather reanalysis products that differ in their biases in temperature and precipitation in the  
307 Thompson Pass region during the winter and the summer seasons. We used the Climate Forecast System Reanalysis version 2  
308 product (CFSv2) and the Modern-Era Retrospective Analysis for Research and Applications version 2 (MERRA2) product for the  
309 weather forcing inputs for SnowModel. The CFSv2 product from the National Centers for Environmental Prediction is an extension  
310 of the lower spatial resolution Climate Forecast System Reanalysis (CFSR) version 1 product that began in 1979 and the version  
311 2 product became available in 2011 (Saha et al., 2010). The CFSv2 data are available at a spatial resolution of 0.2 arc degrees, and  
312 a 6 hour temporal resolution (Saha et al., 2014). The CFSv2 dataset was downloaded using Google Earth Engine (GEE), a platform  
313 for accessing and analyzing scientific datasets with global coverage. The MERRA2 weather reanalysis product from NASA's  
314 Global Modeling and Assimilation office is the second meteorological forcing dataset tested in the present study (Gelaro et al.,  
315 2017). The MERRA2 data are available at a spatial resolution of 0.667 degrees by 0.5 degrees, with a 3 hour temporal resolution  
316 beginning in 1979. MERRA2 replaces the older version product with updated assimilation processes to include more weather  
317 datasets.

### 319 3.4 Snow Datasets

#### 320 3.4.1 Snow Telemetry Station Data

321 The study area contains two SNOTEL stations operated by NRCS. The first station is the Upper Tsaina SNOTEL (UTS) station  
322 located at 534 m.a.s.l. on the NE side of Thompson Pass reporting the full standard set of sensor variables, including precipitation,



326 temperature, snow depth, and SWE. The second station is the Sugarloaf Mountain SNOTEL (SLS) station, located near the Valdez  
327 Arm of the Prince William Sound at 168 m a.s.l. in the SW corner of the study area and records only precipitation, temperature,  
328 and snow depth, but not SWE (Figure 1). The SLS station data was used to create local temperature lapse rates for the calibration  
329 and the UTS station data was used in the manuscript results section to create the SWE time series analysis. Detailed information  
330 about the SNOTEL sensors and climate monitoring instruments can be found at the SNOTEL website  
331 (<https://www.wcc.nrcs.usda.gov/snow/>) and Serreze et al. (1999). Direct links to the SNOTEL websites for the UTS and SLS  
332 stations can also be found in [Section 10](#) below.  
333

Deleted: the Data Availability

Deleted: s

### 334 3.4.2 LiDAR and Photogrammetry Derived Data

335 An [aerial photogrammetric survey](#) was conducted on April 29, 2017 with a Nikon D800 36.2 megapixel camera [flown on a fixed-](#)  
336 [wing aircraft](#) above a portion of the Thompson Pass study area, see [Figure 1b](#) for location and extent. An onboard Trimble Global  
337 Navigation Satellite System (GNSS) and a base-station were used for positional control. Post-processing was completed with  
338 structure-from-motion software to create a digital surface model (DSM) of the photogrammetry-derived snow surface. An airborne  
339 LiDAR survey was collected on April 7th and 8th, 2018, using a Riegl VUX1-LR laser scanner [flown on a fixed-wing aircraft](#). An  
340 onboard integrated inertial measurement unit (IMU) and GNSS, and a base-station were used to provide positional control for the  
341 LiDAR-derived snow DSM. Both RS datasets were evaluated against a previously collected photogrammetry-derived DSM from  
342 2014 when no snow was present. An interpolation scheme was used to gap-fill some of the negative values in the snow DSM due  
343 to vegetation cover effects. There is uncertainty associated with the RS dataset acquisitions, and the sources of error are related to  
344 flight trajectory and geometry, laser scan angle, density of vegetation and canopy, and steep gradients in the terrain (Deems and  
345 Painter, 2006). The vertical RMSE in snow depth for the photogrammetry and LiDAR datasets are estimated at 31.0 cm and 10.2  
346 cm, respectively. While we acknowledge and report these error estimations, they are integrated into the results in Table 3 in Section  
347 [6.5](#) but not used in the spatial results reported in Section 6.2.  
348

Deleted: irborne

Deleted: y

Deleted: and

Deleted: 3

Deleted: 4

### 349 3.4.3 Chugach 2018 Fieldwork Data

350 Three weeks of fieldwork in the Thompson Pass region were conducted in March, April, and May of 2018. Snow depth and SWE  
351 were measured throughout the study area with an avalanche probe and a Federal Snow Sampler. At each fieldwork measuring site,  
352 a central SWE measurement was taken using the Federal Sampler. Avalanche probes were used in the surrounding 100 m<sup>2</sup> to take  
353 a series of 8 snow depth measurements extending 5 m in each direction from the central SWE measurement. Federal sampler data  
354 collection introduces uncertainty in the form of measurement error due to variable snow conditions and densities, hard impenetrable  
355 crusts, and loss during extraction. Dixon and Boon (2012) report the results of several studies showing that the Federal Sampler  
356 error, as a percentage of SWE depth, ranges from 4.6% to 11.2%. Our results presented in Section [6.5](#) include field measurements  
357 of SWE that use the higher 11.2% value for conservative SWE error estimation.  
358

Deleted: 4

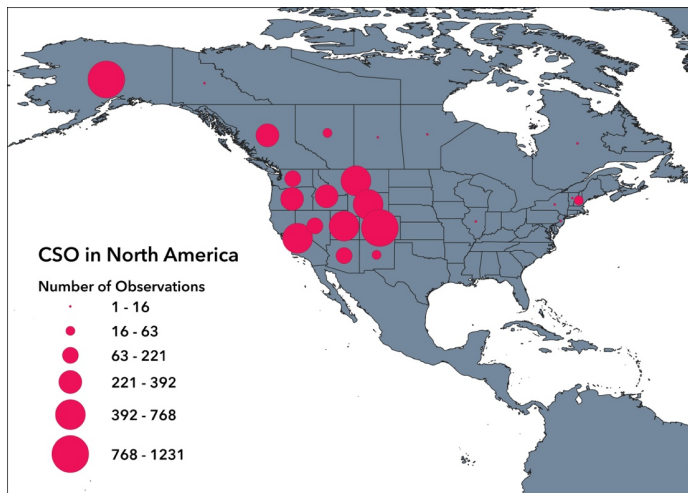
359 The fieldwork sampling protocol was designed to consider: (1) variability in snow depth in small areas less than 100 m<sup>2</sup>, (2) month-  
360 to-month changes in snow depth and SWE, and (3) spatial gradients in snow density throughout the entire study area. A diagram  
361 of the location of each observational site can be found in [Figure 1b](#). The 2018 fieldwork dataset was used for validation with two

Deleted: 3

371 purposes in mind. First, the 2018 fieldwork SWE measurements were used as a validation dataset for the 2018 SWE distribution  
 372 results. Secondly, since the data collected in the spring of 2018 contains measured snow depths and SWE at 70 observational sites  
 373 (n = 560; 8 per site), we conducted an analysis of the sub-grid scale variability in snow depth found at each observational site and  
 374 these results are found in the discussion section.

### 376 3.4.4 Community Snow Observations Data

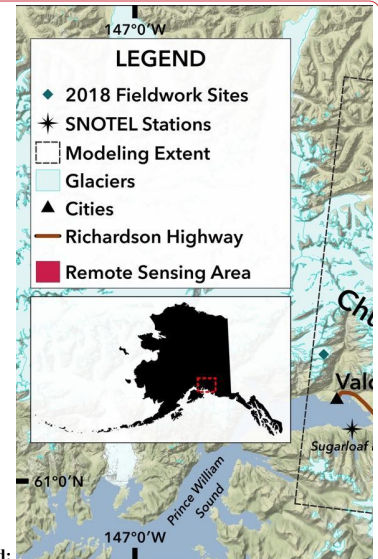
377 The CSO program collects snow depth data from citizen scientists in snowy environments worldwide. Full details including links  
 378 to smartphone apps and tutorials are found at <http://communitysnowobs.org>. Citizen scientists take several (2 to 4) snow depth  
 379 measurements within a small area (< 4 m<sup>2</sup>) using an avalanche probe or other depth measuring device (meterstick, etc.). These  
 380 measurements are then averaged by the participant and submitted using the app or program preferred by the participant. The  
 381 submitted data include the global positioning system (GPS) location in latitude and longitude, time and date, and snow depth  
 382 measurement (cm). The accuracy of the GPS system for each participants' mobile device determines the location error of the GPS,  
 383 with common errors for mobile phones ranging between ±4 to 7 m (Garnett and Stewart, 2015; Schaefer & Woodyer, 2015). Since  
 384 the model resolution is 30 m and 100 m, this level of horizontal error in GPS location is acceptable for the purposes of our research  
 385 questions. All collected data are made freely available on the CSO website for visualization and download (see Section 9 for Data  
 386 Availability). Thousands of measurements have been recorded by participants in CSO globally since it began in January 2017 with  
 387 initial measurement campaigns in Alaska and other frequently visited locations in mountain regions across North America (Figure  
 388 3). In the modeling domain of the current study, 442 CSO measurements were available for WY2017 and 104 CSO measurements  
 389 for WY2018. These measurements were concentrated in the Thompson Pass region of the study area (Figure 1) and range from 25  
 390 m to 1400 m in elevation.



392

Deleted: ¶

Moved up [1]: The 2018 fieldwork includes 72 sites with water equivalent and snow depth measurements. The remote sensing datasets from 2017 and 2018 are overlain on the map, along with the location of the Upper Tsaina and Sugarloaf SNOTEL stations.¶



Deleted: Figure 3: Validation Datasets Map. ¶  
 The 2018 fieldwork includes 72 sites with co-located snow water equivalent and snow depth measurements. The remote sensing datasets from 2017 and 2018 are overlain on the map, along with the location of the Upper Tsaina and Sugarloaf SNOTEL stations.¶

Formatted: Space After: 0 pt, Line spacing: 1.5 lines, Keep with next, Border: Top: (No border), Bottom: (No border), Left: (No border), Right: (No border), Between : (No border)

Deleted: Figure 4

407 **Figure 3: CSO Participation in North America.**  
 408 **Participation in the Community Snow Observations (CSO) project in North America aggregated by the number of observations**  
 409 **recorded in each U.S. state or Canadian province between January 1<sup>st</sup>, 2017 and December 31<sup>st</sup>, 2019.**

Deleted: 4

411 **4 Calibration**

412 We performed model calibration using five years of the historical record of the UTS station from WY2012 through the end of  
 413 WY2016. The calibration was focused on adjustments to temperature lapse rates, precipitation lapse rates, wind adjustment factors,  
 414 and use of the SnowTran3d sub-model. We chose temperature lapse rates and precipitation lapse rates for calibration because  
 415 SnowModel is known to be limited by these factors when large elevational differences exist within the model domain (Liston and  
 416 Elder, 2006a). We chose wind adjustment factors and the wind transportation sub-model for calibration because wind redistribution  
 417 of snow plays a significant role in the study area based on the 2018 fieldwork and the RS surveys from 2017 and 2018. Since the  
 418 SnowAssim sub-model requires a single layer snowpack, no adjustments were made to the snowpack layer structure. For each  
 419 weather reanalysis product, a full calibration was performed for the 30m and 100m model resolutions, in the event that spatial  
 420 resolution plays a significant role in parameter selection. See Appendix A for the descriptions of the model parameters tested  
 421 during the calibration.

422  
 423 The daily SWE output from each calibration simulation is compared with the UTS observed SWE for the duration of the 5-year  
 424 calibration time period using root mean squared error (RMSE), the Nash Sutcliffe Efficiency (NSE), the Kling-Gupta Efficiency  
 425 (KGE), and mean bias error (Bias) to assess the calibration simulations. Table 1 lists the best 30m and 100m calibration simulations,  
 426 based on their time-series RMSE, NSE, KGE, and Bias scores. We acknowledge that measurement errors can occur with SNOTEL  
 427 snow pillows and that these well-known errors may affect the accuracy of the observational dataset (Johnson and Schaeffer, 2002;  
 428 Johnson, 2003).

Deleted:

430 **Table 1: Model Calibration Results.**  
 431 **The best calibration results are given for each set of simulations for water years 2012-2016, along with the root mean squared error**  
 432 **(RMSE), the Nash Sutcliffe Efficiency (NSE), the Kling-Gupta Efficiency (KGE), and the mean bias error (Bias).**

Reanalysis Product & Resolution	Time Step	Number of Simulations	RMSE SWE (cm)	NSE	KGE	Bias SWE (+/- cm)
MERRA2, 30m	3hrly	45	24	-0.29	0.08	+16
MERRA2, 100m	3hrly	45	26	-0.10	-0.10	+19
CFSv2, 30m	6hrly	45	22	-0.15	-0.01	+17
CFSv2, 100m	6hrly	45	22	-0.15	-0.01	+17

433  
 434 Calibration results in Table 1 show that the 30m model grid resolution slightly outperforms the 100m model grid resolution in the  
 435 MERRA2-forced calibration simulations. However, the CFSv2-forced simulations show no difference between the model grid  
 436 resolutions. The CFSv2 product slightly outperforms the MERRA2 product in terms of SWE RMSE. Overall, the differences  
 437 between the top performing model grid resolution and reanalysis product are mixed and potentially negligible, varying by metric.  
 438 The NSE and KGE model performance metrics in the calibration simulations are lower than expected, due primarily to precipitation

441 inputs from the reanalysis products that were consistently higher than measured precipitation at the UTS station (see the following  
442 paragraph for more details). The SnowModel default parameter values notably and consistently produce the top performing  
443 simulations, see Appendix B for details. Due to each of these factors, the calibrated model for the remainder of the study uses the  
444 CFSv2 reanalysis product, the 30m model grid resolution, and the SnowModel default parameter values.

Deleted: Since SnowAssim adjusts the precipitation fields during assimilation, these input deficiencies are acceptable for the purposes of this study.

445  
446 One of the primary obstacles for process modeling is the availability of accurate weather input data, and the related uncertainties  
447 with weather inputs are a well-known complication in snow and hydrological modelling (Rivington et al., 2006; Schmucki et al.,  
448 2014; Schlögl et al., 2016). Initial tests of modeled precipitation fields using Micromet versus the observed precipitation at the  
449 UTS station revealed that both reanalysis products overestimated the amount of precipitation observed in the study area at the UTS  
450 station, see Appendix C. The CFSv2 precipitation totals at the UTS station were nearly 1.6 times the measured precipitation at the  
451 UTS station during the calibration period. The improvements that could be gained by adjusting a subset of the model parameters  
452 (wind, temperature, and precipitation lapse rates due to differences in elevation and season) during calibration were not likely to  
453 overcome this extreme precipitation deficiency, explaining why the final calibrated NSE and KGE values were low. There are two  
454 ways to address this precipitation deficiency using SnowAssim. One is to adjust the precipitation inputs during calibration, and the  
455 other is to allow the assimilation to adjust the precipitation inputs. Both ways are functionally equivalent because they apply a  
456 simple, scalar-based correction surface to the precipitation fluxes. In our calibration process we chose to use SnowAssim to address  
457 the precipitation deficiencies in the reanalysis product, following the approach of other recent studies in mountainous regions of  
458 Alaska, and following the original purpose of the SnowAssim model (Cosgrove et al., 2021, their Calibration of SnowModel  
459 section; Liston and Heimstra, 2008; Young et al., 2020, their section 3.4). This calibration decision supports the primary goal of  
460 the current study, which is to test whether or not participant-submitted snow depth measurements can improve physically-based  
461 modeling efforts through data assimilation.

Deleted: use

462  
463 These calibration results and the precipitation deficiencies motivated us to design an experiment to supplement the main findings  
464 of this research. For this experiment we introduced a model precipitation adjustment factor similar to the method outlined in  
465 Mernild et al. (2006). We applied this scalar value to the precipitation fields as a bias correction of the precipitation inputs. We  
466 tested 11 precipitation adjustment factors ranging from 0.95 to 0.45 and applied them to the meteorological forcing inputs during  
467 the 5-year calibration time period. For more details about the precipitation and precipitation adjustment factor results, see Appendix  
468 D. This experiment, with summary results presented in section 6.6, allows us to test improvements in model performance when the  
469 precipitation inputs are bias corrected prior to model assimilation of CSO measurements.

Deleted: With these obstacles in mind,

Deleted: we

Deleted: ed

Deleted: 5

## 471 472 5 Experimental Design

Deleted: ¶

473 We carried out a series of simulations in order to (1) quantify the improvement in model performance due to the assimilation of  
474 CSO measurements and to (2) understand the effects of the number of CSO data points selected for assimilation. First, we set up  
475 geographic and temporal requirements for the assimilated data. The only geographic requirement was that the CSO measurements  
476 must be located within the larger 5,736 km<sup>2</sup> model domain. We subset the CSO measurements temporally to the peak SWE time  
477 period or later. According to the UTS station, peak SWE in the study area generally occurs mid- to late-April and consequently the

487 earliest assimilation date was set to April 15th. The CSO measurements were aggregated by week by assuming all measurements  
488 in a given week occurred on the same day for the purposes of assimilation. This weekly aggregation allows the correction surfaces  
489 generated by SnowAssim time to adjust the precipitation fluxes and snowmelt factors between observations, thereby altering the  
490 model outputs during assimilation. Additionally, CSO participation in the Thompson Pass region during the early accumulation  
491 season was infrequent in WY2018 and non-existent in WY2017. Since peak SWE is important for mountain hydrology and  
492 ecology, with many snow studies using it as an indicator metric, the time restrictions are acceptable for the research questions  
493 addressed in this study (Bohr and Aguado, 2001; Trujillo et al., 2012; Kapnick and Hall, 2012; Mote et al., 2018; Wrzesien et al.,  
494 2017).

Formatted: Font: Not Bold

496 With these geographic and temporal filters defined for assimilation, we decided to vary the number of CSO data points selected  
497 for assimilation. Model simulations without CSO measurements provide a baseline for comparison, referred to as the NoAssim  
498 case. Ensemble model simulations were carried out with various numbers of CSO measurements assimilated, referred to as the  
499 CSO simulation case. An ensemble of 60 trials per year were carried out with n = 1, n = 2, n = 4, n = 8, n = 16, and n = 32, where  
500 n equals the number of CSO measurements assimilated per WY. In each instance (n value), 10 realizations of the numerical  
501 experiment were carried out. With the ensemble model simulations defined in terms of the spatial and temporal restrictions, the  
502 number of CSO measurements was the only feature modified during assimilation.

Deleted: With the model calibrated, we carried out a series of simulations in order to (1) quantify the improvement in model performance due to the assimilation of CSO measurements and to (2) understand the effects of the number of CSO data points selected for assimilation. Model simulations without CSO measurements provide a baseline for comparison, referred to as the NoAssim case. Ensemble model simulations were also carried out with various numbers of CSO measurements assimilated, referred to as the CSO simulation case. An ensemble of 60 trials per year were carried out with n = 1, n = 2, n = 4, n = 8, n = 16, and n = 32, where n equals the number of CSO measurements assimilated per WY. In each instance (n value), 10 realizations of the numerical experiment were carried out.

Formatted: English (US)

Formatted: Font: Not Bold

## 504 6 Results

505 The following results reflect the three types of available validation datasets: 1) time-series SWE results at the UTS station, 2)  
506 spatial snow depth distributions from the RS datasets, and 3) point-based snow depth and SWE measurements from the 2018  
507 fieldwork.

Deleted:

The timeframe of assimilating CSO measurements was restricted to the peak SWE period or later. According to the UTS station, peak SWE in the study area generally occurs mid- to late-April and consequently the earliest assimilation date was set to April 15<sup>th</sup>. The CSO measurements were aggregated by week because initial simulations suggested that daily increments were not producing realistic results by SnowAssim. Additionally, CSO participation in the Thompson Pass region during the early accumulation season was infrequent in WY2018 and non-existent in WY2017. Since peak SWE is important for mountain hydrology and ecology, with many snow studies using it as an indicator metric, the time restrictions are acceptable for the research questions addressed in this study (Bohr and Aguado, 2001; Trujillo et al., 2012; Kapnick and Hall, 2012; Mote et al., 2018; Wrzesien et al., 2017).

Deleted:

### 509 6.1 Temporal Results Using the Upper Tsaina SNOTEL Station

510 The temporal results compare the UTS station SWE time-series to the ensemble member SWE time-series during WY2017 and  
511 WY2018. Figure 4 displays the temporal cycle of snowpack accumulation and ablation, and the timing of peak SWE. At the UTS  
512 station in the study area, the average WY day of peak SWE is 228, or April 15<sup>th</sup>. Before this day, the snowpack is generally  
513 increasing in SWE and afterwards the snowpack generally enters the ablation period with a reduction in SWE. This temporal cycle  
514 can be observed in Figure 4 by following the color gradient. The highest performing (Best) CSO simulation (Figure 4b,e) corrects  
515 the slope of the snowpack accumulation and ablation phases when contrasted with the NoAssim accumulation and ablation phases  
516 and slopes (Figure 4a,d). These time-series results, in terms of model performance metrics and the snowpack temporal cycle,  
517 exhibit SnowAssim's ability to incorporate CSO measurements and improve modeled SWE outputs at the UTS station location  
518 throughout the entire snow season.

Deleted: Figure 5

Deleted: Figure 5

Deleted: Figure 5

Deleted: Figure 5

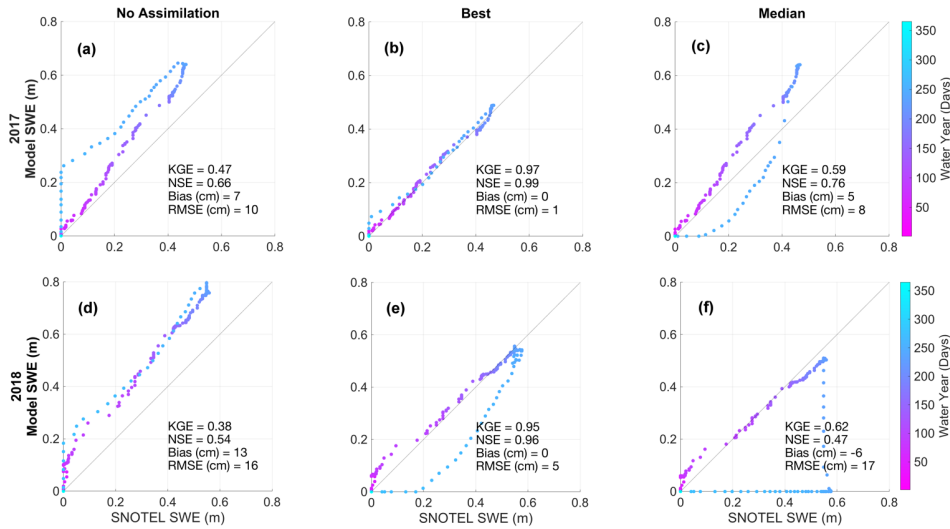


**Figure 4: Time Series at Upper Tsaina SNOTEL Station.**

The Upper Tsaina SNOTEL snow water equivalent (SWE) observations versus the modeled SWE for the no assimilation case (a,d), the Best CSO simulation (b,e), and the Median CSO simulation (c,f). The timeseries color gradient corresponds to the day of the water year.

Deleted: 5

Figure 4 summarizes the temporal results for the Best and median performing (Median) CSO simulations, as well as the NoAssim case. Each ensemble member is evaluated by their KGE, NSE, RMSE, and Bias scores. For results presented in this section, the KGE score is used to rank the ensemble simulations. A full accounting of each ensemble member and their time-series ranking can be found in Appendix E. Modeled SWE depths for the NoAssim case are consistently higher than the UTS station SWE observations for both WYs (Figure 4a,d). The modeled SWE depths for the Best CSO simulation outperform the NoAssim case throughout the entirety of the time-series and represent an improvement in model performance scores according to all of the time-series metrics (Figure 4b,e). The modeled SWE depths for the Median CSO simulation for WY2017 outperform the NoAssim case by all metrics, and the WY2018 Median CSO results are mixed. The ensemble simulation KGE scores outperform the NoAssim KGE scores among 70% of the WY2017 ensemble members, and among 67% of the WY2018 ensemble members. Any number of CSO measurements assimilated show improvements in model performance, a key finding in the time-series results.

Deleted: Figure 5

Deleted: including

Deleted: Figure 5

Deleted: Figure 5

Using the snow depth to SWE conversion method during assimilation introduces uncertainty into the modeling process. Instead of using the global estimates of error reported in Hill et al. (2019; RMSE in SWE = 5.9 cm) we decided to calculate this source of error using our fieldwork site measurements. The RMSE in SWE due to the conversion method is 10.5 cm and we perturbed the CSO observations by this amount to depict the upper and lower boundaries of error associated with this source of uncertainty.

Figure 5 displays the Best CSO simulation temporal results for each WY, along with the UTS station SWE record and the NoAssim case. These perturbations to the assimilated SWE show improved modeled SWE values at the UTS station when compared to the NoAssim case, even after this source of uncertainty has been accounted for.

Deleted: Figure 6

586

587

588

589

590

591

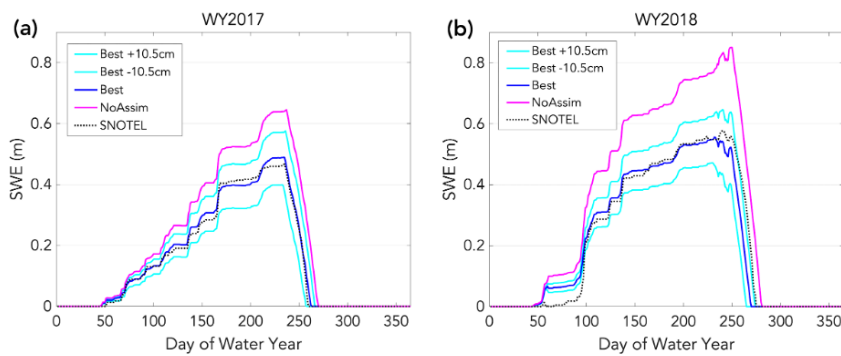
592

593

594

Since the timing of snow disappearance is important for ecological systems in alpine environments and water resources managers, we calculated the range in snow disappearance dates from the Best simulations from both water years (see Figure 5 where SWE depth reaches zero between day 250 and 280). In WY2017 and WY2018, the snow disappearance date for the NoAssim case is 10 and 7 days later than the UTS station record, respectively. In WY2017, the snow disappearance date in the Best CSO simulation, accounting for measurement uncertainty, ranges from 3 days earlier to 8 days later than the UTS station. In WY2018, the range is from 10 days to 1 day earlier than the UTS station. These ranges in snow disappearance date are acceptable and show improvements in model performance for some, but not all, of the Best CSO simulations after accounting for measurement uncertainty.

Deleted: Figure 6



595

596

597

598

**Figure 5:** Snow water equivalent (SWE) time series results with measurement uncertainty included. The simulations with  $\pm 10.5$  cm of SWE represent the upper and lower boundaries of error introduced when converting snow depth measurements to SWE using the Hill et al. (2019) method.

Deleted: 6

599

### 6.2 Spatial Results Using the Remote Sensing Datasets

600

601

602

603

604

605

606

607

608

609

610

611

612

613

The ensemble results are summarized in Figure 6 using the Kolmogorov-Smirnov statistic (KS; Massey, 1951). The KS statistic quantifies the difference between a reference dataset of a continuous variable and a sample dataset of the same variable. The KS statistic represents the maximum distance between the empirical cumulative distribution function (ECDF) of the reference and sample datasets, with KS scores ranging from zero to one, with zero representing perfect dataset agreement (Riemann et al., 2010). In the KS analysis, the reference dataset is the RS derived snow depth distribution and the sample datasets are each of the ensemble snow depth distributions, including the NoAssim case. Figure 6 shows that in WY2017 the CSO simulations are an improvement from the 2017 NoAssim case among 62% of the ensemble members, and in WY2018 among 78% of the ensemble members. Note that only the KS values that fall below the NoAssim line represent an improvement in model performance during the CSO simulations. The spatial results reveal that improvements in model performance are not dependent upon the number of CSO measurements that are assimilated in WY2018. However, WY2017 has a smaller range in KS values as the number of assimilated measurements increases, with more CSO simulations outperforming the NoAssim case. However, WY2017 has a smaller range in KS values as the number of assimilated measurements increases. Additionally, the number of simulations that outperform the NoAssim case in WY2017 gradually increases as the number of CSO measurements increases from 1 to 32. These results also vary according to model performance metric and by WY, with no clear pattern emerging from the number of measurements assimilated.

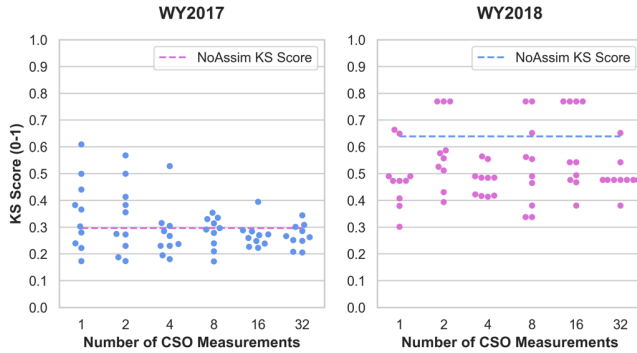
Deleted: Figure 7

Deleted: Figure 7

Formatted: Font: Not Bold

Deleted: .

Formatted: English (US)



620

621

622

623

624

**Figure 6: Swarmplots of Kolmogorov-Smirnov Scores.**  
 The ensemble simulations are ranked by Kolmogorov-Smirnov (KS) score per year and plotted according to the number of measurements assimilated, including the no assimilation (NoAssim) case.

Deleted: 7

625

626

627

628

629

630

631

632

633

634

635

636

The snow depth distribution maps in [Figure 7](#) display the RS datasets (a,b), the results from the [Best](#) CSO simulation (c,d), and the NoAssim case for each WY (e,f). Refer to [Figure 1](#) for the RS dataset location within the study area. We present the Best CSO simulation as the focus of Section 6.2 ranked according to KS score ranking ([Figure 6](#)). A full accounting of each ensemble member and their spatial distribution ranking can be found in Appendix F. In the RS datasets, there is more variation and heterogeneity in snow depth across short distances ([Figure 7a-b](#)). This spatial diversity is evident even after the RS dataset has been aggregated to correspond to the model resolution at 30 m, as depicted in [Figure 7](#). The NoAssim case and Best CSO simulation show less spatial diversity, and the NoAssim case broadly overestimates snow depth when compared to the Best CSO simulation for both WYs. The visualization of the snow depth distributions in [Figure 7](#) illustrates the challenges of accurately representing the process scale through physics-based modeling at low resolutions (Blöschl, 1999), and some of these challenges will be examined further in the discussion section.

Deleted: Figure 8

Deleted: highest performing

Deleted: 2

Deleted: Figure 7

Deleted: Figure 8

Deleted: Figure 8

Deleted: Figure 8

Deleted: Figure 8



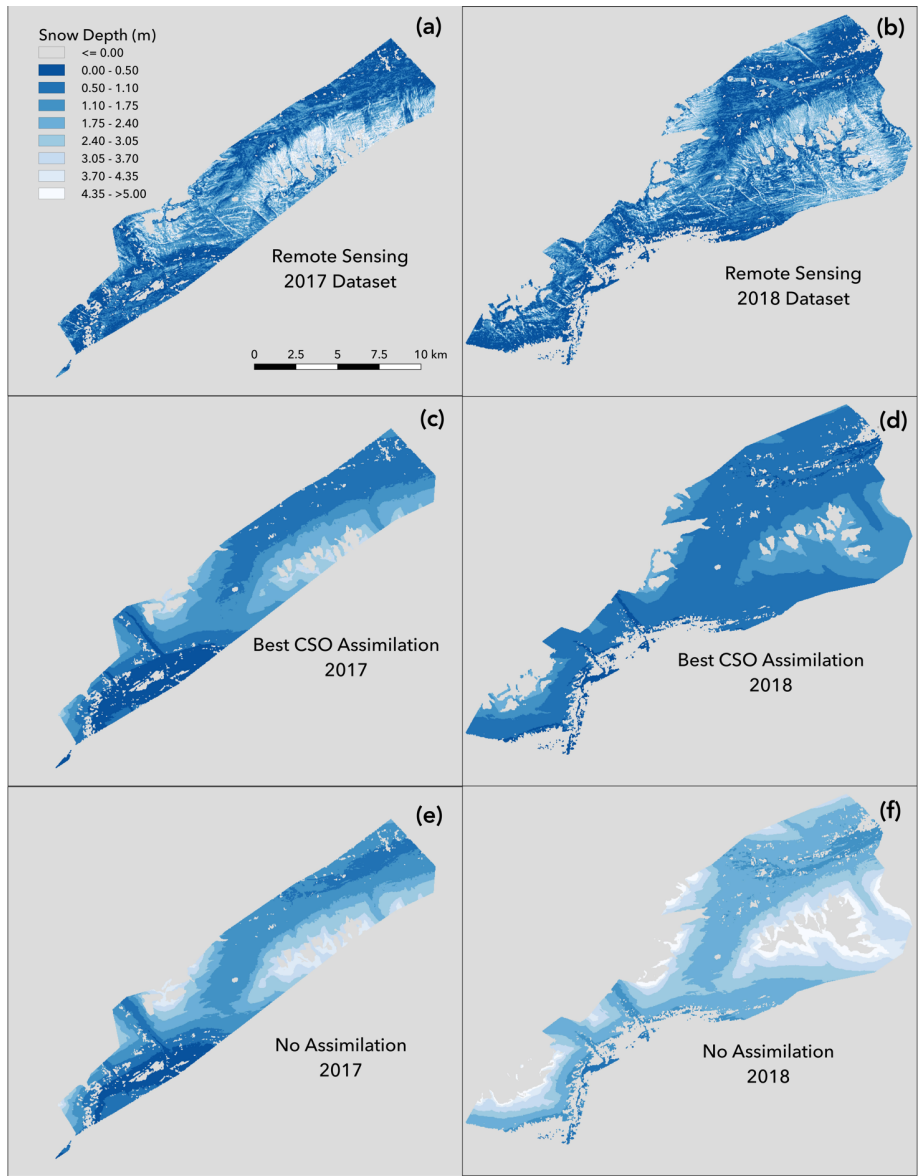


**Figure 7: Snow Depth Distribution Maps.**

(a,b) The remote sensing (RS) datasets from 2017 and 2018. (c,d) The best CSO simulation results corresponding to the RS dataset spatial extent. (e,f) The no assimilation results corresponding to the RS dataset spatial extent. The total model area that corresponds to the RS dataset in 2017 is 104 km<sup>2</sup> and 149 km<sup>2</sup> in 2018.

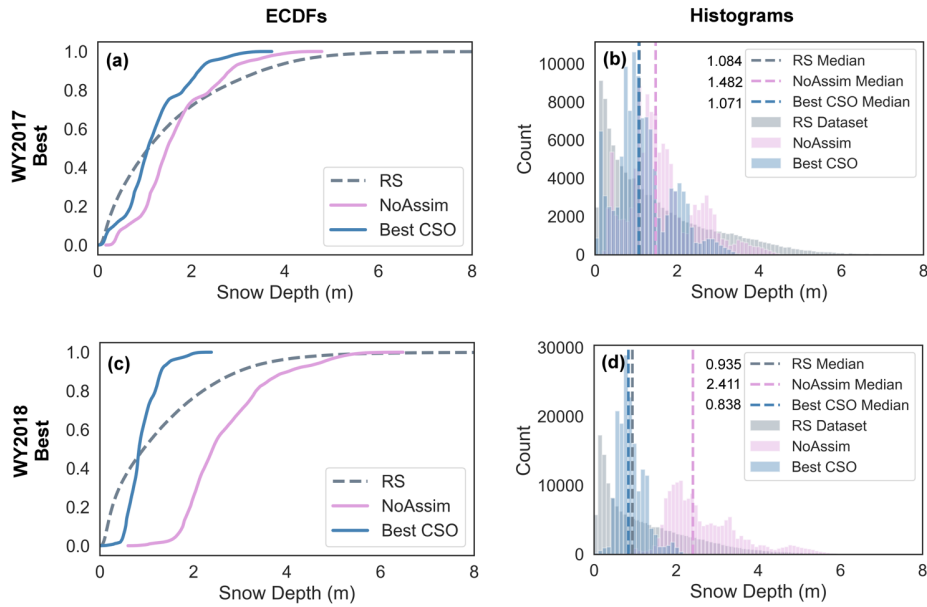
Deleted: 8

645  
646  
647  
648  
649

651

652 [Figure 8](#) presents histograms and empirical cumulative distribution functions (ECDFs) for the RS datasets, the NoAssim case, and  
 653 the Best CSO simulation. In WY2017 ([Figure 8a](#)), when the NoAssim case overestimates snow depths, the Best CSO simulation  
 654 ECDF shifts left, towards the RS dataset ECDF. To a greater degree, in WY2018 ([Figure 8c](#)) when the NoAssim case more broadly  
 655 overestimates the snow depths, the Best CSO simulation ECDF shifts further left, towards the RS dataset ECDF. The shifts in the  
 656 ECDFs are evident in the histograms and the median value of each dataset is indicated with a dashed line ([Figure 8b,d](#)). The same  
 657 shifts are evident in the snow depth distribution maps ([Figure 7c,d,e,f](#)). Even though the shifts in ECDFs and histograms are in the  
 658 correct direction in the Best CSO simulations, SnowAssim is not adjusting the distribution of snow depth values, which can be  
 659 seen in the multimodal shape of the histograms.  
 660

Deleted: Figure 9  
 Deleted: Figure 9  
 Deleted: Figure 9  
 Deleted: Figure 9  
 Deleted: Figure 8



661

662 **Figure 8: Histogram and Distribution Plots.**  
 663 The empirical cumulative distribution functions (ECDFs) and histograms from the best CSO simulation, the no assimilation case, and  
 664 the remote sensing (RS) datasets during WY2017 (a,b) and WY2018 (c,d).

Deleted: 9

665

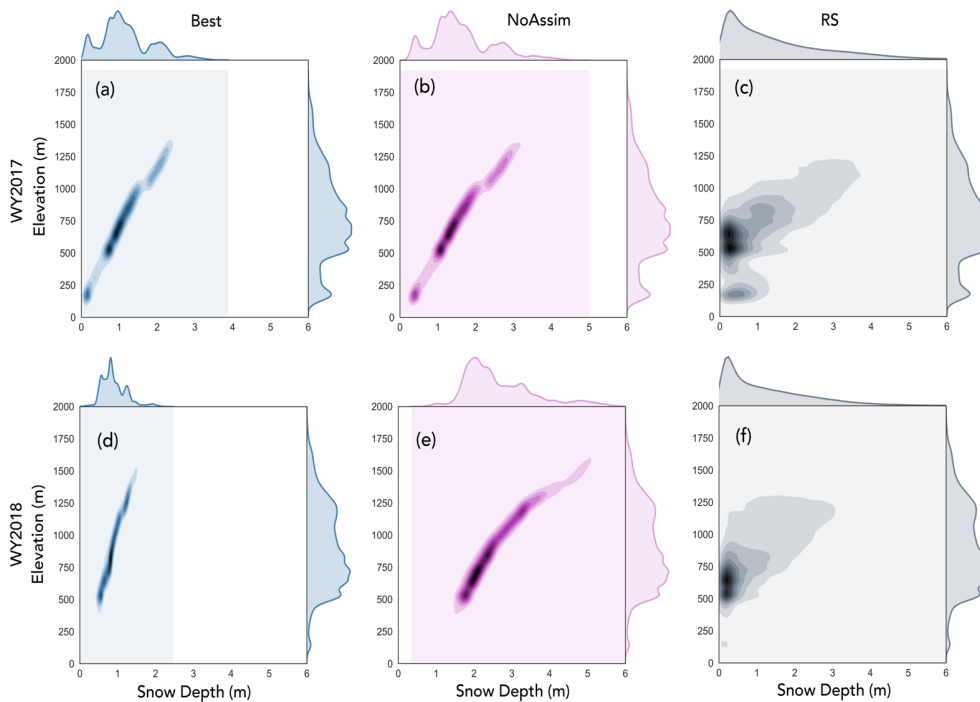
666 The multimodal distribution of snow depths in the modeled results can be explained by their relationship to the elevation of the  
 667 surrounding terrain. The input DEM and the snow depth distributions were compared on a grid-cell-to-grid-cell basis using a two-  
 668 dimensional histogram (2DH). [Figure 9](#) is a series of 2DHs that display snow depth (x axes) versus the input DEM (y axes) in the  
 669 RS area from both years. Darker colors indicate a higher frequency of snow depth and elevation values corresponding to each  
 670 dataset. The 2DHs show a proportional relationship between the modeled snow depths ([Figure 9a,b,e,f](#)) and the input DEM values.  
 671 As elevation increases, snow depth also increases linearly in the modeled results. Still, the range of snow depths from Best CSO

Deleted: Figure 10

Deleted: Figure 10

680 simulation shifts towards the RS dataset in both years, but the elevation relationship remains largely intact. The RS snow depths  
 681 are less dependent on elevation, with snow depth values between 0 and 1 appearing at all elevations between 0 and 1250m. The  
 682 2DH analysis supports the findings from the snow depth distribution maps where the variability of snow depth observed in the RS  
 683 dataset is not replicated in the NoAssim case or the Best CSO simulation (Figure 7).  
 684

Deleted: Figure 8



685 **Figure 9: Two-dimensional Histograms.**

686 The remote sensing (RS) dataset vs. the (a) water year (WY) 2017 no assimilation case, (b) WY2018 no assimilation case, (c) WY2017  
 687 best CSO simulation, and (d) WY2018 best CSO simulation.  
 688

Deleted: 10

Deleted: ¶

### 689 6.3 Spatial and Temporal Characteristics of the Assimilated Data

690 The geographic locations of the CSO measurements used in the temporal and spatial results are an important factor that can shed  
 691 some light on our understanding of the assimilation process. First, the time-series analysis validation metrics were quantified for  
 692 all days in the water year at the UTS location. The CSO measurements that were assimilated in 2017 range in distance from 4.1  
 693 km to 30.5 km away from the UTS location, while the Best CSO simulation measurements (n=2) were located 5.5 and 6.9 km  
 694 away. In 2018 the assimilated measurements range in distance from 2.1 km to 17.4 km away from the UTS location, and the Best  
 695 CSO simulation measurements (n=2) were located 9.1 and 17.5 km away. Figure 10 includes a map of the assimilated  
 696 measurements and a histogram of the distance between the CSO measurements and the UTS station from both water years,  
 697 subset by the assimilation time period (on or after April 15th of each year). This distance analysis demonstrates that the CSO

Formatted: Font: Not Bold

Formatted: Left

Formatted: Font: Not Bold

Formatted: Font: Not Bold

measurements used in the time-series assimilation do not coincide with the SNOTEL grid cell location. The histogram shows that improvements made at the SNOTEL location during assimilation were due to snow depth measurements taken by CSO participants kilometers away.

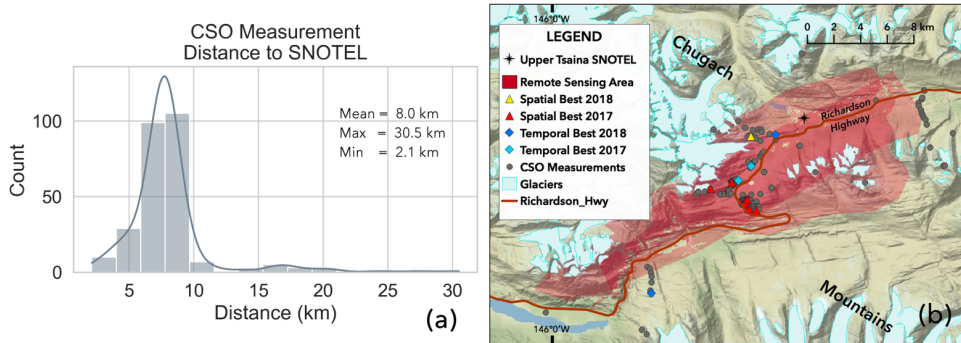


Figure 10: Assimilated measurements.

Formatted: Centered

(a) A histogram showing the distance between the CSO measurements available for assimilation and the Upper Tsaina SNOTEL station, subset by the assimilation time period, on or after April 15<sup>th</sup> (n=266). A kernel density estimator is used to smooth the distribution. (b) A map of the CSO measurement locations that includes the best spatial and temporal CSO simulations for both water years. The map is zoomed in on the area of the highest density of CSO measurements.

Formatted: Superscript

Secondly, the remote sensing datasets were collected on April 29th in 2017 and April 7th and 8th in 2018. These validation datasets are essentially a spatial snapshot of snow depth from a single day in both water years. In water year 2017, there were a total of 9 CSO measurements submitted on April 29th, the same day as the remote sensing dataset collection. For the presented results in Section 6.2, none of these 9 CSO measurements from April 29th were used. For water year 2018, the remote sensing dataset was collected on April 8th and the measurements were not assimilated temporally until at least April 15th (see the experimental design outlined in Section 5). Figure 10b displays the locations of the CSO measurements assimilated in the Best CSO simulation from both water years (WY2017 n=1; WY2018 n=8). This analysis of the assimilated data demonstrates that the CSO measurements used in the spatial assimilation do not coincide with the dates of the remote sensing acquisition, revealing that improvements were made during assimilation by measurements that were taken at a different time.

Formatted: Justified

#### 6.4.2018 Fieldwork Results

Deleted: 3

To validate the WY2018 SWE distributions from the NoAssim case and the Best CSO simulation we used ground-truth data from our field campaign in April 2018. The locations of the 70 SWE and snow depth measurement sites from 2018 are depicted in Figure 1b. Figure 11 shows the co-located SWE depth measurements (y axes) versus the snow depth measurements (x axes) from each site aggregated by month. The bars in Figure 11 represent the variability in snow depth within the surrounding 100m<sup>2</sup> of the SWE measurement, including the average, minimum, and maximum of 8 snow depth measurements at each site. Table 2 shows the results at the SWE measurement sites, comparing the NoAssim case versus the Best CSO simulation using RMSE, bias, and mean absolute error (MAE) metrics for evaluation. Since each measurement site corresponds to a single CSO snow depth

Deleted: Fieldwork

Deleted: 3

Deleted: Figure 11

Deleted: Figure 11

735 submission, we separated those measurement sites used in the assimilation scheme from the validation set when creating Table 2.  
 736 The Best CSO simulation outperforms the NoAssim case according to all metrics in all months. The 2018 fieldwork results from  
 737 April show that the Best CSO simulation has a bias of +3 cm, while the NoAssim case is +97 cm. The April 2018 fieldwork results  
 738 agree with the histogram and ECDF analysis that displayed broad overestimation of SWE in the NoAssim case in WY2018 (Figure  
 739 7b; Figure 8d).

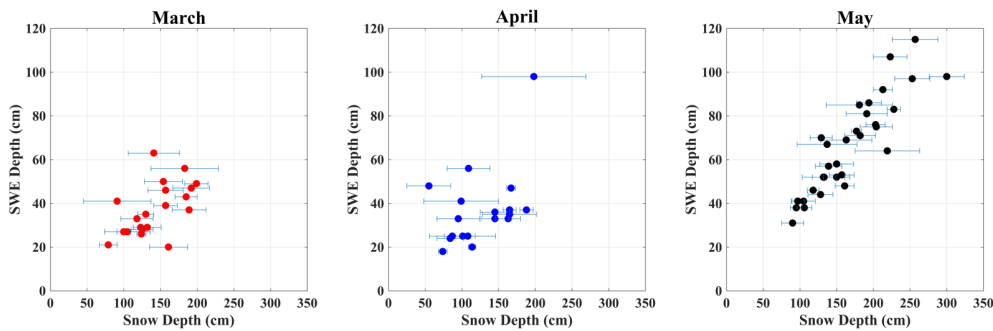
Deleted: Figure 8

Deleted: Figure 9

741 Additionally, we used the co-located snow depth and SWE measurements at the fieldwork sites to quantify the uncertainty that is  
 742 added to the model during the snow depth to SWE conversion. By converting the fieldwork snow depth values to SWE using the  
 743 Hill et al. (2019) method, we can compare the measured SWE to the approximated SWE values. The fieldwork measured mean  
 744 SWE is 51 cm, the RMSE in SWE is 10.5 cm, and the Bias in SWE is 0.6 cm when using the Hill method for all fieldwork sites.

Deleted: ment

Deleted:



746

Figure 11: Fieldwork 2018 Measurements by Month

747 The 70 *in-situ* snow water equivalent (SWE) measurements (y axes) from 2018 are plotted by month along with their co-located snow  
 748 depth measurements (x axes). The bars show the minimum, maximum, and average of each fieldwork site where 8 snow depth  
 749 measurements were obtained in a 100 m<sup>2</sup> area.

Deleted: 1

Table 2: Fieldwork 2018 Results

751 The 70 SWE measurements from the 2018 fieldwork compared to the Best CSO simulation and the no assimilation (NoAssim) case  
 752 using the three model performance metrics: root mean squared error (RMSE), mean bias error (Bias), and mean absolute error  
 753 (MAE).  
 754

	Bias SWE (cm)		RMSE SWE (cm)		MAE SWE (cm)	
	Best CSO	NoAssim	Best CSO	NoAssim	Best CSO	NoAssim
All	-11	86	28	100	22	86
March	-3	77	15	95	13	77
April	3	97	21	114	16	97
May	-25	84	37	95	31	84

755

756 **6.5 Spatially Averaged Snow Water Equivalent Results**

Deleted: 4

757 Another way to quantify the ability of CSO measurements to constrain SnowModel output is to investigate the modeled SWE  
 758 averaged over a large area. Table 3 contains the spatially averaged SWE estimations from the RS survey area in WY2018, and

765 includes the RS dataset, the Best CSO simulation, and the NoAssim case. We focus on WY2018 because the fieldwork  
 766 measurements include estimated bulk density values at each measurement site. These bulk density estimations were measured  
 767 during April 2018 and were partitioned from the larger dataset and spatially averaged over the RS region only (n=22). The  
 768 fieldwork estimated bulk density value was then applied to the spatially averaged RS snow depth. The uncertainty estimations for  
 769 the RS survey dataset and the Federal Sampler collected data are also added to Table 3 to create a range of estimation of water  
 770 volume. For the Best CSO simulation and the NoAssim case, the spatially averaged snow depth, SWE, and snow density values  
 771 were taken directly from the model results. The SWE estimation results in Table 3 demonstrate that SnowAssim can constrain the  
 772 SWE output over a large region based on a few, randomly chosen CSO measurements. Importantly, the accuracy of the total  
 773 modeled water volume from the RS region in 2018 improves when CSO measurements are included, a key finding that has  
 774 implications for water resource management decisions in snowy, data-limited, mountain environments.

775

776

777

778

779

**Table 3: Spatially Averaged Variables in the RS Region**  
 The spatially averaged results were calculated using the RS region in WY2018, the RS dataset ( $\pm 1\text{cm}$  error), the spatially averaged  
 density, and the modeled results. The spatially averaged SWE depth for the RS survey was estimated using the average density ( $\pm$   
 11.2%) measured during April 2018 fieldwork.

Dataset	Spatially Averaged Snow Depth (cm)	Spatially Averaged Density (kg/m <sup>3</sup> )	Spatially Averaged SWE Depth (cm)	Total RS Region Water Volume (km <sup>3</sup> )
RS Survey 2018	130 $\pm$ 1 (RS survey)	331 $\pm$ 37 (fieldwork)	38 - 48 (estimated)	0.06 – 0.07 (estimated)
Best CSO Simulation 2018	130 (modeled)	400 (modeled)	52 (modeled)	0.08 (modeled)
NoAssim 2018	267 (modeled)	430 (modeled)	115 (modeled)	0.17 (modeled)

780

781 **6.6. Precipitation Adjustment Experiment**

782 The experimental design of the present study was developed for remote locations where a long-term precipitation dataset was not  
 783 available to bias correct the precipitation inputs. However, since a long-term precipitation dataset may be available in other  
 784 locations, we decided to test the results with a precipitation experiment. In this experiment we applied a scalar to the CFSv2  
 785 precipitation fields for bias correction and all other model parameters and input datasets were held constant. The experiment results  
 786 show that some of the CSO ensemble simulations still outperformed the NoAssim case with the precipitation adjustment, both  
 787 spatially and temporally. For example, the spatial results show that 43% percent of the ensemble runs in WY2017 and 20% of the  
 788 ensemble runs in WY2018 outperformed the NoAssim case when the precipitation was bias corrected, according to their KS score  
 789 (Figure 12). Similarly, the temporal results show that 42% of the ensemble runs in WY2017 and 58% of the ensemble runs in  
 790 WY2018 outperformed the NoAssim case when the precipitation was bias corrected, according to their KGE score. The ECDF  
 791 and histogram analysis from the precipitation adjustment factor experiment also show model improvements when there was broad  
 792 underestimation of snow depths in the NoAssim case in WY2017 and broad overestimation in WY2018. These results demonstrate  
 793 that using CSO measurements for assimilation can improve model performance when the available weather forcing dataset has  
 794 known biases (no precipitation adjustment factor case) but when those biases have been decreased (precipitation adjustment factor  
 795 case) the improvements become less clear, they vary from year to year, and are less consistent between spatial and temporal results.

796

Deleted:   
 Deleted: 5

Deleted: Figure 12

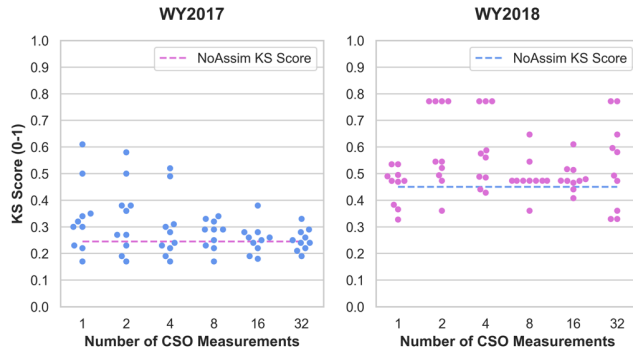


Figure 12: Swarmplots of Kolmogorov-Smirnov Scores with Precipitation Adjustment Factor.

The ensemble simulations are ranked by Kolmogorov-Smirnov (KS) score per water year (WY) and plotted according to the number of CSO measurements assimilated, including the no assimilation (NoAssim) case.

Deleted: Figure 1  
Deleted: 2

### 6.7. Correction Factor Results

SnowAssim generates a set of correction factors for each of the CSO ensemble member simulations. These factors correspond to the observed and measured differences in the SWE variable and are used to create a correction surface with the Barnes objective analysis. Table 4 reviews a subset of the correction factors, including data from the Best ranked CSO simulations according to the various temporal and spatial metrics previously reviewed in sections 6.1 and 6.2. The number of observations varies for the Best ranked simulation, as well as the precipitation correction factors, the use of a melt correction factor, and whether an interpolated correction surface was created. These correction factor results show that relatively few measurements are needed during assimilation and that there are multiple paths to improving model performance when assimilating CSO observations using SnowAssim.

Deleted: 6

Deleted: or not

Table 4: Correction factors from the assimilation scheme for the best ranked simulations from both water years. The model determination for precipitation vs melt correction factors is included and whether the Barnes objective analysis created a spatially distributed correction surface.

Deleted: or not

Type	Ranking	Year	# of Obs	Precipitation Correction Factors	Melt Correction Factors (-)	Interpolated Surface?	Dates
Temporal	Best	2017	2	0.45, 1.04	n/a	Yes	4/29/17
Temporals	Best	2018	2	0.68, 0.76	n/a	Yes	5/15/18
Spatial	Best	2017	8	0.30, 0.50, 0.73, 0.86, 1.36	6.32, 2.29, 22.6	Yes	4/29/17; 5/8/17
Spatial	Best	2018	1	0.32	n/a	No	5/22/18

825 **7 Discussion**

826 An important consideration in the results of the present study involves ranking the CSO ensemble members by various spatial and  
827 temporal metrics. The time series results (Section 6.1), the spatially distributed results (Section 6.2), and the spatially averaged  
828 results (Section 6.5) did not have the same ranking order for the CSO ensemble members. For example, the Best CSO simulation  
829 in WY2017 from the time-series analysis was an ensemble member with two CSO measurements assimilated according to the  
830 KGE metric. The time-series results represent a single point in the domain at the UTS station. By contrast, the Best CSO simulation  
831 in WY2017 from the spatial distribution analysis was an ensemble member with eight CSO measurements assimilated using the  
832 KS score. The spatially distributed results represent the entire RS survey area. The improvements in model performance are  
833 determined by the type of validation dataset available and the metric used to quantify those improvements. In other words, one  
834 size does not fit all when it comes to quantifying improvements to model performance using CSO measurements.

835  
836 The variability of snow depth and SWE in mountain catchments and the spatial patterning of snowpack conditions in complex  
837 terrain is a well-known challenge in snow modeling and snow remote sensing research (Anderton et al., 2004; López-Moreno et  
838 al., 2013; Luce et al., 1998; Molotch et al., 2005; Rice and Bales, 2010; Sturm and Wagner, 2010b). The RS results reveal that  
839 variability in snow depth across short distances is largely a function of wind redistribution and drifting and not primarily a function  
840 of elevation (Figure 8c,f; Figure 6a,b). Thompson Pass is a notoriously windy location, and the RS dataset shows complex drifting  
841 patterns throughout the surveyed area (Figure 6a,b). The wind inputs from the reanalysis product used in Micromet and  
842 SnowTran3d may not be adequate for the steepness and ruggedness of the terrain. Although wind scaling factors were tested in the  
843 calibration, the only suitable calibration dataset was the SNOTEL site. SNOTEL stations are often situated in locations where the  
844 effects of wind redistribution of the snowpack are minimal, and SNOTEL station data are often not representative of the spatial  
845 variability of the surrounding areas (Dressler et al., 2006; Molotch and Bales, 2005). The inability of SnowTran3d to resolve the  
846 wind redistribution of the snowpack more accurately, the coarse wind field inputs from the reanalysis products, and the use of a  
847 single SNOTEL station for calibration, together represent a model and input data limitation of the current study.

848  
849 The ensemble results highlight a broader issue in snow hydrology and process modeling in general, regarding the sub-grid scale  
850 variability of the modeled state variable within a single model grid cell. The scale of the *in-situ* observations (measured with an  
851 avalanche probe) and the scale of the model resolution (30 m grid) versus the scale of the physical process being modeled (true  
852 patterns and true variance in space and time) can create scale effects that need to be accounted for (Blöschl et al., 1999). In this  
853 way, the 2018 fieldwork has a significant role to play in our understanding of the sub-grid scale variability in snow depth  
854 distributions. CSO participants average a few point measurements over a 1 to 4 m<sup>2</sup> area. The model resolution is 30 m, or 900 m<sup>2</sup>  
855 per grid model grid cell. If participants move slightly one direction or another, their averaged and submitted measurements would  
856 likely be different, but their measurements would potentially lie within the same 30 m model grid cell. This difference, in turn,  
857 would modify the SWE depth inputs for SnowAssim. To better characterize the sub-grid scale variability of snow depth we  
858 investigate the 8 avalanche probe depths taken over 100 m<sup>2</sup> at each of the 70 observation sites during the 2018 fieldwork (see also  
859 Figure 11). From these data, a picture of the sub-grid scale variability emerges. The largest range in snow depth values at a single  
860 100 m<sup>2</sup> observation site is 2.11 m and the smallest range in snow depth values at a single site is 0.09 m. The highest standard  
861 deviation (sd) found at a single observation site is 0.71 m and the lowest sd is 0.04 m. This shows that a significant amount of  
862 variation, and therefore uncertainty, is being added to the model chain simply by the sub-grid scale variability of snow depth

Deleted: 4

Deleted: Figure 9

Deleted: Figure 7

Deleted: Figure 7

Deleted: dampened

Deleted: deeper question

Deleted: Figure 11



870 distributions within a single model grid cell, distributions that the model will not be able to resolve at the low model spatial  
871 resolution. Sub-grid scale variability is a well known problem in snow science and represents a limitation of the improvements that  
872 can be made by assimilating CSO measurements (Blöschl and Kirnbauer, 1993; Elder et al., 1998; Liston and Hiemstra, 2008;  
873 Schmucki et al., 2013).

874

875 One of the limitations of the present study is that the physical and temporal characteristics of the CSO measurements like aspect,  
876 elevation, and early-season measurements were not fully analyzed. Initial simulations demonstrated that SnowAssim performs best  
877 when the assimilated measurements were located close in time to the validation dataset. This factor influenced our choice to focus  
878 on the late-season time period of CSO measurements since the RS surveys were conducted in the late-season. Additionally, since  
879 the majority of the CSO measurements for both WYs occurred between March 15<sup>th</sup> and May 15<sup>th</sup>, future research should be in a  
880 location where CSO measurements are obtained frequently throughout the accumulation season. A research project with many  
881 measurements throughout the accumulation period may provide more insights into the temporal aspects of assimilation of CSO  
882 measurements. We decided not to subset the CSO measurements by geophysical characteristics like aspect, elevation, and land  
883 cover type because these require additional analysis that is outside of the scope of the current study. Understanding the effects of  
884 temporal and spatial restrictions of CSO measurements on model performance will likely be an area of future research.  
885 Additionally, it may be necessary to test other process models and alternate assimilation schemes in the future to improve the  
886 spatial distribution of model results and determine if CSO measurements can be used in other modeling contexts.

887

## 888 **8 Conclusions**

889 In this study we use a new snow dataset collected by participants in the Community Snow Observations (CSO) project in coastal  
890 Alaska to improve snow depth and snow water equivalence (SWE) outputs from a snow process model. Ensemble simulations  
891 were carried out during the 2017 and 2018 snow seasons to investigate the effects of incorporating citizen science measurements  
892 into the model chain using an assimilation scheme. Time series SNOTEL station records, remotely sensed photogrammetry and  
893 light detection and ranging surveys, and fieldwork observations are used to validate the modeled snow depth and snow water  
894 equivalent distributions. Any number of CSO measurements assimilated improves model performance, from 1 to 32. Our results  
895 demonstrate that using CSO measurements for assimilation can improve model performance when the available weather forcing  
896 dataset has known biases and also when those biases have been decreased by using a precipitation adjustment factor. The  
897 improvements in model performance from CSO measurements occur in 62% to 78% of the ensemble simulations both spatially  
898 and temporally, and in cases when the model broadly overestimates or underestimates snow depth and SWE. Model estimations  
899 of total water volume from a sub-region of the study area also demonstrate improvements in accuracy after CSO measurements  
900 have been assimilated. This study has implications for water resource management and snow modeling in locations where *in-situ*  
901 snow information is limited but snow enthusiasts often visit, since even small numbers of assimilated CSO measurements can  
902 improve the snow model outputs.

903

904

Deleted: tested

Deleted: 7

907 **9. Appendices**

Deleted: 8

908

**Appendix A: Model calibration parameters and their descriptions.**

Parameter	# of Options	Format	Description
Temperature Lapse Rate	3 sets	Monthly	PRISM Climatologies; Local Weather Station Data; SnowModel Default
Precipitation Lapse Rate	5 sets	Monthly	Monthly Coefficients of 1/4, 1/2, 3/4, 1 (SnowModel Default), PRISM Climatologies
Wind Adjustment Factor	3	Coefficient	Coefficients of 1 (SnowModel Default), 2, 3
SnowTran3d	2	On/Off	

909

910

911

**Appendix B: Top performing parameter configurations from the calibration simulations.**

Rank	Temperature Lapse Rate	Precipitation Scaling Factor	Wind Adjustment Factor	SnoTran on/off
Tied for first	Default	Default	Default	On
Tied for first	Local Weather Station	Default	Default	On
Tied for first	PRISM Climatologies	Default	Default	On

912

913

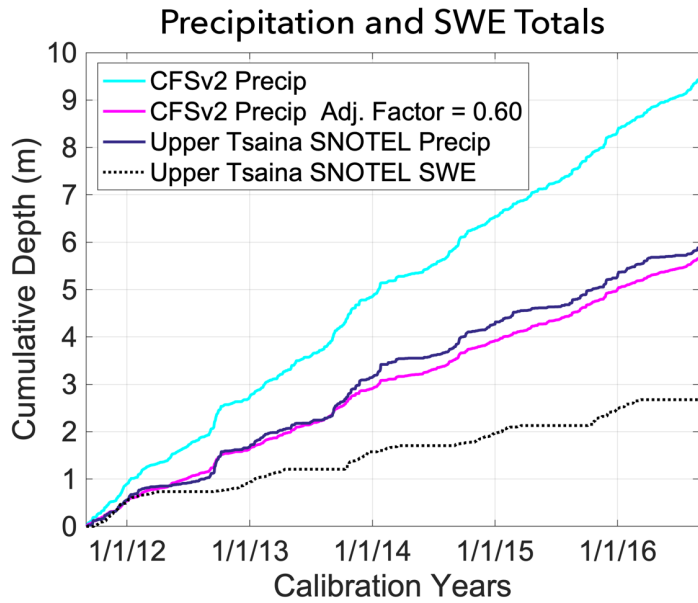
914

915

916

917

**Appendix C: Precipitation totals at the Upper Tsaina SNOTEL station compared to the CFSv2-forced model totals and the CFSv2-forced model totals with a precipitation adjustment factor. This overestimation of precipitation by the reanalysis product is a major factor in the quality of the calibration results.**



918

920  
921  
922  
923

**Appendix D: Precipitation Adjustment Factor Results.**

The best precipitation adjustment factors are shown, along with the root mean squared error (RMSE), the Nash Sutcliffe Efficiency (NSE), the Kling-Gupta Efficiency (KGE), and the mean bias error (Bias).

Reanalysis, Resolution	Time		Number of Simulations	Precipitation	RMSE			Bias
	Period (WY)	Time Step		Adjustment Factor	Precipitation (mm)	NSE	KGE	Precipitation (+/- mm)
MERRA2, 30m	2012-2016	3hrly	11	0.55	7.5	0.07	0.20	0.0
MERRA2, 100m	2012-2016	3hrly	11	0.55	7.5	0.07	0.20	0.0
CFSv2, 30m	2012-2016	6hrly	11	0.60	6.7	0.27	0.35	-0.1
CFSv2, 100m	2012-2016	6hrly	11	0.60	6.7	0.27	0.35	-0.1

924  
925  
926  
927  
928  
929

**Appendix E: Ranked Temporal Results.**

Ensemble results from ranked by Kling-Gupta efficiency (KGE) score for water year (WY) 2017 (a) and WY2018 (b). Also included are the Nash Sutcliffe Efficiency (NSE) and the mean bias error (Bias) values.

(a) WY2017

Rank	Number of CSO Measurements	Iteration	KGE	NSE	Bias (cm)
1	2	2	0.97	0.99	0
2	1	8	0.97	0.99	0
3	4	1	0.94	0.93	0
4	2	6	0.93	0.92	0
5	8	9	0.93	0.89	-1
6	16	8	0.90	0.84	-1
7	32	3	0.88	0.96	-1
8	4	4	0.88	0.91	-2
9	1	10	0.80	0.95	-3
10	4	3	0.80	0.89	2
11	16	2	0.78	0.82	-3
12	8	1	0.77	0.81	2
13	32	8	0.77	0.79	-3
14	2	8	0.77	0.93	-3
15	16	7	0.76	0.93	-3
16	16	1	0.75	0.87	-3
17	4	6	0.74	0.92	-3
18	1	6	0.71	0.89	4
19	16	3	0.67	0.88	-4
20	32	4	0.66	0.79	-5
21	32	5	0.65	0.78	-5
22	32	1	0.65	0.78	-5
23	32	7	0.64	0.80	-5
24	2	3	0.63	0.80	4
25	4	9	0.62	0.83	-5
26	16	9	0.62	0.82	-5
27	2	10	0.61	0.82	-5
28	16	4	0.60	0.75	-5
29	32	6	0.59	0.82	-5
30	8	8	0.59	0.76	5
31	32	2	0.57	0.78	6
32	16	5	0.56	0.73	-6
33	4	8	0.56	0.73	-6

34	8	10	0.55	0.72	-6
35	8	7	0.54	0.73	-6
36	16	6	0.54	0.70	-6
37	1	3	0.54	0.74	6
38	8	2	0.52	0.68	-6
39	8	4	0.52	0.71	-6
40	1	2	0.51	0.72	-6
41	4	10	0.50	0.67	-7
42	32	10	0.49	0.66	-7
43	4	7	0.46	0.63	-7
NoAssim	NoAssim	NoAssim	0.47	0.66	7
44	8	3	0.43	0.66	-7
45	32	9	0.41	0.63	-8
46	8	5	0.39	0.54	-8
47	2	1	0.36	0.53	-8
48	8	6	0.34	0.49	-9
49	1	4	0.33	0.49	-9
50	1	7	0.29	0.42	-9
51	2	4	0.28	0.41	-9
52	16	10	0.26	0.37	-10
53	2	5	0.22	0.32	-10
54	1	5	0.17	0.23	-11
55	1	9	0.08	0.05	-12
56	2	7	0.08	0.05	-12
57	4	2	0.06	0.02	-12
58	4	5	0.03	-0.03	-12
59	2	9	-0.02	-0.13	-13
60	1	1	-0.07	-0.24	-14

930  
931

(b) WY2018

Rank	Number of CSO Measurements	Iteration	KGE	NSE	Bias (m)
1	2	7	0.95	0.96	0
2	8	9	0.91	0.90	2
3	8	5	0.90	0.89	2
4	2	9	0.88	0.91	2
5	2	4	0.87	0.93	-2
6	4	7	0.87	0.97	3
7	4	8	0.84	0.97	-2
8	1	5	0.84	0.95	-2
9	1	6	0.84	0.95	-2
10	4	10	0.82	0.95	4
11	2	2	0.77	0.92	5
12	4	9	0.77	0.88	-4
13	16	9	0.76	0.85	-4
14	16	5	0.76	0.53	-2
15	16	4	0.76	0.53	-2
16	4	6	0.75	0.84	-4
17	32	10	0.74	0.49	-2
18	4	5	0.71	0.72	-5
19	2	6	0.71	0.89	6
20	1	8	0.71	0.83	-5
21	1	1	0.71	0.83	-5
22	1	9	0.71	0.83	-5
23	8	7	0.69	0.80	-6
24	16	8	0.68	0.58	-6
25	16	2	0.65	0.77	-6
26	32	2	0.65	0.53	-6
27	32	5	0.64	0.50	-6
28	32	8	0.64	0.49	-6
29	32	7	0.62	0.47	-6

30	32	9	0.62	0.47	-6
31	32	4	0.62	0.46	-6
32	32	1	0.62	0.46	-6
33	8	10	0.57	0.42	-7
34	4	1	0.53	0.65	-9
35	2	1	0.52	0.65	-9
36	32	3	0.49	0.18	6
37	4	4	0.48	0.60	-10
38	4	2	0.47	0.60	-10
39	4	3	0.45	0.57	-10
40	8	6	0.43	0.52	11
41	2	3	0.38	0.46	-11
42	1	7	0.33	0.38	-12
43	8	4	0.30	0.29	-13
44	1	2	0.30	0.36	15
45	16	1	0.24	0.14	-14
46	32	6	0.24	0.13	-14
47	1	4	0.23	0.29	16
48	1	10	0.07	-0.09	-17
49	8	8	0.01	-0.21	-18
50	8	3	0.00	-0.24	-18
51	1	3	-0.07	-0.37	-20
52	16	3	-0.15	-1.18	18
53	16	7	-0.16	-1.15	18
54	16	6	-0.16	-1.15	18
55	8	1	-0.16	-1.14	18
56	16	10	-0.16	-1.13	19
57	2	8	-0.23	-1.05	21
58	8	2	-0.28	-1.07	23
59	2	5	-0.37	-1.18	27
60	2	10	-0.58	-2.00	32

932

933

934

935

936

937

Appendix F: Ranked Spatial Results.

Spatial distribution ensemble results ranked by Kolmogorov-Smirnov (KS) score for water year (WY) 2017 (a) and WY2018 (b). Also included are the root mean squared error (RMSE) and the median values.

(a) WY2017 Results

Rank	Number of CSO Measurements	Iteration	KS Score (0 - 1)	RMSE (m)	Median (m)	Mean (m)
1	8	9	0.17	1.171	1.071	1.198
2	1	8	0.17	1.173	1.066	1.192
3	2	2	0.17	1.173	1.064	1.190
4	4	1	0.18	1.164	1.096	1.225
5	2	6	0.19	1.159	1.116	1.248
6	4	4	0.19	1.202	0.983	1.100
7	32	2	0.21	1.149	1.156	1.393
8	32	3	0.21	1.222	0.931	1.044
9	8	8	0.21	1.148	1.166	1.402
10	1	10	0.22	1.243	0.888	0.995
11	16	8	0.22	1.287	0.693	0.883
12	16	1	0.23	1.251	0.872	0.978
13	2	8	0.23	1.256	0.861	0.966
14	4	2	0.23	1.135	1.250	1.396
15	4	3	0.23	1.135	1.250	1.396
16	4	6	0.24	1.267	0.840	0.942
17	16	7	0.24	1.270	0.834	0.936
18	8	1	0.24	1.133	1.281	1.430
19	1	6	0.24	1.133	1.281	1.430
20	16	2	0.25	1.321	0.651	0.814
21	32	4	0.25	1.293	0.801	0.891

22	32	5	0.25	1.293	0.794	0.892
23	16	3	0.26	1.306	0.770	0.866
24	32	1	0.26	1.310	0.761	0.855
25	32	7	0.27	1.316	0.754	0.847
26	4	9	0.27	1.320	0.749	0.843
27	16	4	0.27	1.324	0.738	0.832
28	2	10	0.27	1.328	0.731	0.825
29	16	9	0.27	1.328	0.730	0.824
30	2	3	0.27	1.135	1.406	1.567
31	8	10	0.28	1.344	0.715	0.804
32	1	3	0.28	1.137	1.426	1.589
33	16	5	0.28	1.349	0.696	0.788
34	4	8	0.29	1.350	0.694	0.786
35	32	6	0.29	1.351	0.692	0.784
36	16	6	0.29	1.355	0.685	0.777
37	8	7	0.29	1.360	0.678	0.769
NoAssim	NoAssim	NoAssim	0.30	1.145	1.482	1.651
38	8	2	0.30	1.370	0.663	0.753
39	32	10	0.30	1.384	0.649	0.731
40	1	2	0.30	1.381	0.644	0.734
41	4	10	0.30	1.384	0.639	0.729
42	32	8	0.31	1.404	0.461	0.667
43	8	4	0.31	1.400	0.614	0.703
44	4	7	0.32	1.402	0.612	0.701
45	8	3	0.33	1.426	0.573	0.662
46	8	5	0.34	1.438	0.565	0.649
47	32	9	0.34	1.448	0.546	0.630
48	8	6	0.35	1.469	0.521	0.603
49	2	1	0.36	1.468	0.514	0.600
50	1	4	0.37	1.484	0.490	0.576
51	1	7	0.38	1.510	0.453	0.539
52	2	4	0.38	1.510	0.453	0.539
53	16	10	0.39	1.529	0.426	0.512
54	2	5	0.41	1.559	0.385	0.472
55	1	5	0.44	1.601	0.330	0.418
56	1	9	0.50	1.684	0.223	0.314
57	2	7	0.50	1.684	0.223	0.314
58	4	5	0.53	1.724	0.175	0.268
59	2	9	0.57	1.770	0.119	0.217
60	1	1	0.61	1.812	0.067	0.173

938  
939  
940  
941  
942

(b) WY2018 Results

Rank	Number of CSO Measurements	Iteration	KS Score (0 - 1)	RMSE (m)	Median (m)	Mean (m)
1	1	10	0.30	1.210	0.838	0.905
2	8	3	0.34	1.246	0.756	0.810
3	8	8	0.34	1.246	0.756	0.810
4	1	7	0.38	1.146	1.124	1.238
5	16	1	0.38	1.150	1.127	1.237
6	32	6	0.38	1.150	1.127	1.237
7	8	4	0.38	1.150	1.127	1.237
8	2	3	0.39	1.146	1.182	1.304
9	1	3	0.41	1.319	0.621	0.655
10	4	3	0.41	1.153	1.261	1.392
11	4	1	0.42	1.147	1.292	1.437
12	4	2	0.42	1.155	1.279	1.413
13	4	4	0.42	1.165	1.305	1.435

14		2	1	0.43	1.166	1.335	1.474
15		8	7	0.46	1.205	1.487	1.651
16		16	2	0.47	1.261	1.568	1.708
17		1	1	0.47	1.221	1.521	1.684
18		1	9	0.47	1.221	1.521	1.684
19		1	8	0.47	1.221	1.523	1.686
20		16	8	0.48	1.233	1.553	1.746
21		32	1	0.48	1.233	1.553	1.746
22		32	2	0.48	1.233	1.553	1.746
23		32	4	0.48	1.233	1.553	1.746
24		32	5	0.48	1.233	1.553	1.746
25		32	7	0.48	1.233	1.553	1.746
26		32	8	0.48	1.233	1.553	1.746
27		32	9	0.48	1.233	1.553	1.746
28		4	9	0.48	1.244	1.577	1.753
29		4	5	0.48	1.248	1.580	1.748
30		4	6	0.48	1.248	1.580	1.748
31		1	5	0.49	1.259	1.607	1.780
32		1	6	0.49	1.259	1.607	1.780
33		4	8	0.49	1.259	1.607	1.780
34		8	10	0.49	1.259	1.607	1.780
35		16	9	0.49	1.281	1.628	1.801
36		2	4	0.51	1.318	1.714	1.893
37		2	7	0.53	1.353	1.777	1.968
38		16	4	0.54	1.401	1.848	2.068
39		16	5	0.54	1.401	1.848	2.068
40		32	10	0.54	1.401	1.848	2.068
41		8	9	0.55	1.453	1.922	2.131
42		4	7	0.55	1.454	1.928	2.132
43		2	9	0.56	1.461	1.939	2.148
44		8	5	0.56	1.500	1.977	2.189
45		4	10	0.56	1.493	1.980	2.191
46		2	2	0.58	1.540	2.043	2.263
47		2	6	0.59	1.606	2.128	2.350
<b>NoAssim</b>	<b>NoAssim</b>	<b>NoAssim</b>		0.64	1.861	2.411	2.678
48		1	2	0.65	1.894	2.436	2.721
49		32	3	0.65	1.928	2.466	2.764
50		8	6	0.65	1.928	2.466	2.764
51		1	4	0.66	2.009	2.567	2.852
52		16	10	0.77	2.932	3.466	3.839
53		16	3	0.77	2.932	3.466	3.839
54		16	6	0.77	2.932	3.466	3.839
55		16	7	0.77	2.932	3.466	3.839
56		2	10	0.77	2.932	3.466	3.839
57		2	5	0.77	2.932	3.466	3.839
58		2	8	0.77	2.932	3.466	3.839
59		8	1	0.77	2.932	3.466	3.839
60		8	2	0.77	2.932	3.466	3.839

943

944 **10. Code and Data Availability**

945 The datasets used in this study can be found at the following locations.

946

- 947 1. Community Snow Observations website and snow depth data download at <http://app.communitysnowobs.org/>  
948 (last accessed 30 April 2020).

949

Deleted: 9

- 951 2. The snow depth to snow water equivalence calculator (Hill et al., 2019) can be downloaded via Github at  
952 <https://github.com/communitysnowobs/snowdensity> (last accessed: 30 April 2020).  
953
- 954 3. Snow Telemetry data for the Upper Tsaina River station near Valdez, Alaska is available at the Natural Resources  
955 Conservation Service website: <https://wcc.sc.egov.usda.gov/nwcc/site?sitenum=1055> (last accessed: 30 April 2020).  
956
- 957 4. Climate Forecast System Reanalysis version 2 (CFSv2) data (Saha et al., 2011) is available for download at  
958 <https://rda.ucar.edu/datasets/ds094.0/#!description>.  
959
- 960 5. The CFSv2 data was accessed using Google Earth Engine at [https://developers.google.com/earth-  
961 engine/datasets/catalog/NOAA\\_CFSV2\\_FOR6H](https://developers.google.com/earth-engine/datasets/catalog/NOAA_CFSV2_FOR6H) (last accessed: 30 April 2020). A javascript version of the Earth Engine  
962 code written for this project is available at [https://github.com/snowmodel-tools/preprocess\\_javascript](https://github.com/snowmodel-tools/preprocess_javascript) (last accessed: 30  
963 April 2020).  
964
- 965 6. To convert the CFSv2 data downloaded from Google Earth Engine to the necessary input file for MicroMet we  
966 wrote Matlab scripts that can be downloaded via Github at [https://github.com/snowmodel-tools/preprocess\\_matlab](https://github.com/snowmodel-tools/preprocess_matlab) (last  
967 accessed: 30 April 2020).  
968
- 969 7. The MERRA2 weather reanalysis product from NASA's Global Modeling and Assimilation office (Gelaro et  
970 al., 2017) can be downloaded at [https://gmao.gsfc.nasa.gov/reanalysis/MERRA-2/data\\_access/](https://gmao.gsfc.nasa.gov/reanalysis/MERRA-2/data_access/) (last accessed: 30 April  
971 2020).  
972
- 973 8. The National Elevation Dataset is (Gesch et al., 2002) available for download at  
974 <https://catalog.data.gov/dataset/usgs-national-elevation-dataset-ned> (last accessed: 30 April 2020).  
975
- 976 9. The National Land Cover Database 2011 dataset (Homer et al., 2011) is available for download at the Multi-  
977 Resolution Land Characteristics Consortium at <https://www.mrlc.gov/data?f%5B0%5D=category%3Aland%20cover>  
978 (last accessed: 30 April 2020).

## 979 **11. Author Contributions**

980 Ryan Crumley, David Hill, Gabriel Wolken, Katreen Wikstrom Jones, and Anthony Arendt designed the research questions and  
981 decided on the methods. Ryan Crumley, Gabriel Wolken, Katreen Wikstrom Jones, Christopher Cosgrove, and David Hill  
982 conducted fieldwork in the study area, including snowpack sampling and remote sensing surveys. Ryan Crumley and Dave Hill  
983 oversaw the analysis of the manuscript. Anthony Arendt designed and maintained the CSO website and snow dataset with  
984 contributions from all authors. Community Snow Observation Participants and all authors contributed snow depth measurements.  
985 Ryan Crumley prepared the manuscript with contributions from all authors during editing and review process.

## 986 **12. Competing Interests**

987 The authors declare that they have no conflicts of interest.

Deleted: 0

Deleted: 1



990 **13. Acknowledgements**

991 This research has been supported by NASA (grant no. NNX17AG67A) and CUAHSI (Pathfinder Fellowship grant). Arendt was  
992 partially supported by the Washington Research Foundation, and by a Data Science Environments project award to the University  
993 of Washington eScience Institute from the Gordon and Betty Moore and the Alfred P. Sloan Foundations. [Los Alamos National  
994 Laboratory has approved the dissemination of this manuscript with the assigned the LA-UR-21-26394 number.](#)  
995

Deleted: 2

996 **References**

997 Anderton, S.P., White, S.M. and Alvera, B.: Evaluation of spatial variability in snow water equivalent for a high mountain  
998 catchment. *Hydrological Processes*, 18(3), pp.435-453, <https://doi.org/10.1002/hyp.1319>, 2004.  
999

Formatted: Font: Not Italic

Formatted: Font: Not Italic

1000 Bales, R.C., Molotch, N.P., Painter, T.H., Dettinger, M.D., Rice, R. and Dozier, J.: Mountain hydrology of the western United  
1001 States. *Water Resources Research*, 42(8), <https://doi.org/10.1029/2005WR004387>, 2006.  
1002

1003 Baba, M., Gascoïn, S., Jarlan, L., Simonneaux, V. and Hanich, L.: Variations of the Snow Water Equivalent in the Ourika  
1004 Catchment (Morocco) over 2000–2018 Using Downscaled MERRA-2 Data. *Water*, 10(9), p.1120,  
1005 <https://doi.org/10.3390/w10091120>, 2018.  
1006

1007 Barnes, S.L.: A technique for maximizing details in numerical weather map analysis, *Journal of Applied Meteorology*, 3(4),  
1008 pp.396-409, [https://doi.org/10.1175/1520-0450\(1964\)003<0396:ATFMDI>2.0.CO;2](https://doi.org/10.1175/1520-0450(1964)003<0396:ATFMDI>2.0.CO;2), 1964.  
1009

1010 Barnes, S.L.: Mesoscale objective map analysis using weighted time-series observations, Technical Report, National Severe  
1011 Storms Lab., Norman, Oklahoma, 1973.  
1012

1013 Barnett, T.P., Adam, J.C. and Lettenmaier, D.P.: Potential impacts of a warming climate on water availability in snow-dominated  
1014 regions. *Nature*, 438(7066), p.303, <https://doi.org/10.1038/nature04141>, 2005.  
1015

1016 Beamer, J.P., Hill, D.F., Arendt, A. and Liston, G.E.: High-resolution modeling of coastal freshwater discharge and glacier mass  
1017 balance in the Gulf of Alaska watershed, *Water Resources Research*, 52(5), pp.3888-3909,  
1018 <https://doi.org/10.1002/2015WR018457>, 2016.  
1019

1020 Beamer, J.P., Hill, D.F., McGrath, D., Arendt, A. and Kienholz, C.: Hydrologic impacts of changes in climate and glacier extent  
1021 in the Gulf of Alaska watershed, *Water Resources Research*, 53, pp.7502-7520, <https://doi.org/10.1002/2016WR020033>, 2017.  
1022

1023 Blöschl, G., Kimbauer, R.: An analysis of snow cover patterns in a small alpine catchment, *Hydrological Processes*, 6(1), pp.99-  
1024 109, <https://doi.org/10.1002/hyp.3360060109>, 1992.  
1025

1026 Blöschl, G.: Scaling issues in snow hydrology. *Hydrological processes*, 13(14-15), pp.2149-2175,  
1027 [https://doi.org/10.1002/\(SICI\)1099-1085\(199910\)13:14/15<2149::AID-HYP847>3.0.CO;2-8](https://doi.org/10.1002/(SICI)1099-1085(199910)13:14/15<2149::AID-HYP847>3.0.CO;2-8), 1999.  
1028

1030 Bohr, G.S. and Aguado, E.: Use of April 1 SWE measurements as estimates of peak seasonal snowpack and total cold-season  
1031 precipitation. *Water Resources Research*, 37(1), pp.51-60, <https://doi.org/10.1029/2000WR900256>, 2001.

1032

1033 Bonney, R., Cooper, C.B., Dickinson, J., Kelling, S., Phillips, T., Rosenberg, K.V. and Shirk, J.: Citizen science: a developing tool  
1034 for expanding science knowledge and scientific literacy. *BioScience*, 59(11), pp.977-984, <https://doi.org/10.1525/bio.2009.59.11.9>,  
1035 2009.

1036

1037 Bühler, Y., Adams, M.S., Bösch, R. and Stoffel, A.: Mapping snow depth in alpine terrain with unmanned aerial systems (UASs):  
1038 potential and limitations. *The Cryosphere*, 10(3), pp.1075-1088, <https://doi.org/10.5194/tc-10-1075-2016>, 2016.

1039

1040 Buytaert, W., Zulkafli, Z., Grainger, S., Acosta, L., Alemie, T.C., Bastiaensen, J., De Bièvre, B., Bhusal, J., Clark, J., Dewulf, A.  
1041 and Foggin, M.: Citizen science in hydrology and water resources: opportunities for knowledge generation, ecosystem service  
1042 management, and sustainable development. *Frontiers in Earth Science*, 2, p.26, <https://doi.org/10.3389/feart.2014.00026>, 2014.

1043

1044 Carroll, T., Cline, D., Fall, G., Nilsson, A., Li, L. and Rost, A.: NOHRSC operations and the simulation of snow cover properties  
1045 for the coterminous US. In *Proc. 69th Annual Meeting of the Western Snow Conf* (pp. 1-14), 2001.

1046

1047 Carrassi, A., Bocquet, M., Bertino, L. and Evensen, G.: Data assimilation in the geosciences: An overview of methods, issues, and  
1048 perspectives. *Wiley Interdisciplinary Reviews: Climate Change*, 9(5), p.e535, <https://doi.org/10.1002/wcc.535>, 2018.

1049

1050 Carter, S., Carter, P. and Levison, J.: Skier triggered surface hoar: A discussion of avalanche involvements during the 2006 Valdez  
1051 Chugach helicopter ski season. In *Proceedings of International Snow Science Workshop* (pp. 860-867), 2006.

1052

1053 Clark, M.P., Slater, A.G., Barrett, A.P., Hay, L.E., McCabe, G.J., Rajagopalan, B. and Leavesley, G.H.: Assimilation of snow  
1054 covered area information into hydrologic and land-surface models. *Advances in water resources*, 29(8), pp.1209-1221,  
1055 <https://doi.org/10.1016/j.advwatres.2005.10.001>, 2006.

1056

1057 Clark, M.P., Hendrikx, J., Slater, A.G., Kavetski, D., Anderson, B., Cullen, N.J., Kerr, T., Örn Hreinsson, E. and Woods, R.A.:  
1058 Representing spatial variability of snow water equivalent in hydrologic and land-surface models: A review. *Water Resources*  
1059 *Research*, 47(7), <https://doi.org/10.1029/2011WR010745>, 2011.

1060

1061 Contosta, A.R., Adolph, A., Burchsted, D., Burakowski, E., Green, M., Guerra, D., Albert, M., Dibb, J., Martin, M., McDowell,  
1062 W.H. and Routhier, M.: A longer vernal window: the role of winter coldness and snowpack in driving spring transitions and lags.  
1063 *Global change biology*, 23(4), pp.1610-1625, <https://doi.org/10.1111/gcb.13517>, 2017.

1064

1065 Cooper, C. B., Dickinson J., Phillips, T., and Bonney, R.: Citizen science as a tool for conservation in residential ecosystems.  
1066 *Ecology and Society* 12(2): 11. URL: <http://www.ecologyandsociety.org/vol12/iss2/art11/> (accessed 05 May 2020), 2007.

1067 ▼ Cosgrove, C.L., Wells, J., Nolin, A.W., Putera, J. and Prugh, L.R.: Seasonal influence of snow conditions on Dall's sheep  
1068 productivity in Wrangell-St Elias National Park and Preserve. *PloS one*, 16(2), p.e0244787, 2021.  
1069

1070

Deleted:

1072 Crumley, R.L., Hill, D.F., Beamer, J.P. and Holzenthal, E.R.: Seasonal components of freshwater runoff in Glacier Bay, Alaska:  
1073 diverse spatial patterns and temporal change. *The Cryosphere*, 13(6), pp.1597-1619, <https://doi.org/10.5194/tc-13-1597-2019>,  
1074 2019.

1075

1076 Deems, J.S. and Painter, T.H.: Lidar measurement of snow depth: accuracy and error sources. In Proceedings of the 2006  
1077 International Snow Science Workshop: Telluride, Colorado, USA, International Snow Science Workshop (pp. 330-338), 2006.

1078

1079 Dickinson, J.L., Zuckerberg, B. and Bonter, D.N.: Citizen science as an ecological research tool: challenges and benefits. *Annual*  
1080 *review of ecology, evolution, and systematics*, 41, pp.149-172, <https://doi.org/10.1146/annurev-ecolsys-102209-144636>, 2010.

1081

1082 Dixon, D. and Boon, S.: Comparison of the SnowHydro snow sampler with existing snow tube designs. *Hydrological Processes*,  
1083 26(17), pp.2555-2562, <https://doi.org/10.1002/hyp.9317>, 2012.

1084

1085 Dressler, K.A., Fassnacht, S.R. and Bales, R.C.: A comparison of snow telemetry and snow course measurements in the Colorado  
1086 River basin. *Journal of hydrometeorology*, 7(4), pp.705-712, <https://doi.org/10.1175/JHM506.1>, 2006.

1087

1088 Elder, K., Rosenthal, W. and Davis, R.E.: Estimating the spatial distribution of snow water equivalence in a montane watershed.  
1089 *Hydrological Processes*, 12(10-11), pp.1793-1808, [https://doi.org/10.1002/\(SICI\)1099-1085\(199808/09\)12:10<1793::AID-  
1090 HYP695>3.0.CO;2-K](https://doi.org/10.1002/(SICI)1099-1085(199808/09)12:10<1793::AID-HYP695>3.0.CO;2-K), 1998.

1091

1092 Fayad, A., Gascoin, S., Faour, G., López-Moreno, J.I., Drapeau, L., Le Page, M. and Escadafal, R.: Snow hydrology in  
1093 Mediterranean mountain regions: A review. *Journal of Hydrology*, 551, pp.374-396, <https://doi.org/10.1016/j.jhydrol.2017.05.063>,  
1094 2017.

1095

1096 Fienen, M.N. and Lowry, C.S.: Social. Water—A crowdsourcing tool for environmental data acquisition. *Computers &*  
1097 *Geosciences*, 49, pp.164-169, <https://doi.org/10.1016/j.cageo.2012.06.015>, 2012.

1098

1099 Fletcher, S.J., Liston, G.E., Hiemstra, C.A. and Miller, S.D.: Assimilating MODIS and AMSR-E snow observations in a snow  
1100 evolution model. *Journal of Hydrometeorology*, 13(5), pp.1475-1492, <https://doi.org/10.1175/JHM-D-11-082.1>, 2012.

1101

1102 Garnett, R. and Stewart, R.: Comparison of GPS units and mobile Apple GPS capabilities in an urban landscape. *Cartography and*  
1103 *Geographic Information Science*, 42(1), pp.1-8, <https://doi.org/10.1080/15230406.2014.974074>, 2015.

1104

1105 Gesch, D., Evans, G., Mauck, J., Hutchinson, J., Carswell Jr., W.J.: The National Map—Elevation: U.S. Geological Survey Fact  
1106 Sheet 2009-3053, 2009.

1107

1108 Gelaro, R., McCarty, W., Suárez, M.J., Todling, R., Molod, A., Takacs, L., Randles, C.A., Darmenov, A., Bosilovich, M.G.,  
1109 Reichle, R. and Wargan, K.: The modern-era retrospective analysis for research and applications, version 2 (MERRA-2). *Journal*  
1110 *of Climate*, 30(14), pp.5419-5454, <https://doi.org/10.1175/JCLI-D-16-0758.1>, 2017.

1111

1112 Haberkorn, A.: European Snow Booklet – an Inventory of Snow Measurements in Europe. *EnviDat*.  
1113 <https://doi.org/10.16904/envidat.59>, 2019.

1114  
1115 Hall D.K., Riggs G.A., Salomonson V.V.: MODIS/Terra Snow Cover Daily L3 Global 500m Grid, Version 6. Boulder, CO: NASA  
1116 National Snow and Ice Data Center Distributed Active Archive Center, 2016.  
1117  
1118 Han, E., Merwade, V. and Heathman, G.C.: Implementation of surface soil moisture data assimilation with watershed scale  
1119 distributed hydrological model. *Journal of hydrology*, 416, pp.98-117, <https://doi.org/10.1016/j.jhydrol.2011.11.039>, 2012.  
1120  
1121 Hedrick, A.R., Marks, D., Havens, S., Robertson, M., Johnson, M., Sandusky, M., Marshall, H.P., Kormos, P.R., Bormann, K.J.  
1122 and Painter, T.H.: Direct insertion of NASA Airborne Snow Observatory-derived snow depth time series into the iSnobal energy  
1123 balance snow model. *Water Resources Research*, 54(10), pp.8045-8063, <https://doi.org/10.1029/2018WR023190>, 2018.  
1124  
1125 Helmert, J., Lange, M., Dong, J., De Rosnay, P., Gustafsson, D., Churulin, E., Kurzeneva, E., Müller, R., Trentmann, J., Souverijns,  
1126 N. and Koch, R.: 1st Snow Data Assimilation Workshop in the framework of COST HarmoSnow ESSEM 1404. *Meteorologische*  
1127 *Zeitschrift*, 27(4), pp.325-333, <https://doi.org/10.1127/metz/2018/0906>, 2018.  
1128  
1129 Hendriks, J., Johnson, J. and Shelly, C.: Using GPS tracking to explore terrain preferences of heli-ski guides. *Journal of outdoor*  
1130 *recreation and tourism*, 13, pp.34-43, <https://doi.org/10.1016/j.jort.2015.11.004>, 2016.  
1131  
1132 Hill, D., Wolken, G., Wikstrom Jones K., Crumley, R., and Arendt, A.: Crowdsourcing snow depth data with citizen scientists,  
1133 *Eos*, 99, <https://doi.org/10.1029/2018EO108991>, 2018.  
1134  
1135 Hill, D.F., Burakowski, E.A., Crumley, R.L., Keon, J., Hu, J.M., Arendt, A.A., Wikstrom Jones, K. and Wolken, G.J.: Converting  
1136 snow depth to snow water equivalent using climatological variables. *The Cryosphere*, 13(7), pp.1767-1784, <https://doi.org/10.5194/tc-13-1767-2019>, 2019.  
1137  
1138  
1139 Holko, L., Gorbachova, L. and Kostka, Z.: Snow hydrology in central Europe. *Geography Compass*, 5(4), pp.200-218,  
1140 <https://doi.org/10.1111/j.1749-8198.2011.00412.x>, 2011.  
1141  
1142 Homer, C., Dewitz, J., Yang, L., Jin, S., Danielson, P., Xian, G., Coulston, J., Herold, N., Wickham, J. and Megown, K.:  
1143 Completion of the 2011 National Land Cover Database for the conterminous United States—representing a decade of land cover  
1144 change information. *Photogrammetric Engineering & Remote Sensing*, 81(5), pp.345-354, [https://doi.org/10.1016/S0099-1112\(15\)30100-2](https://doi.org/10.1016/S0099-1112(15)30100-2), 2015.  
1145  
1146  
1147 Jonas, T., Marty, C. and Magnusson, J.: Estimating the snow water equivalent from snow depth measurements in the Swiss Alps.  
1148 *Journal of Hydrology*, 378(1-2), pp.161-167, <https://doi.org/10.1016/j.jhydrol.2009.09.021>, 2009.  
1149  
1150 Johnson, J.B.: A theory of pressure sensor performance in snow. *Hydrological Processes*, 18(1), pp.53-64,  
1151 <https://doi.org/10.1002/hyp.1310>, 2003.  
1152  
1153 Johnson, J.B. and Schaefer, G.L.: The influence of thermal, hydrologic, and snow deformation mechanisms on snow water  
1154 equivalent pressure sensor accuracy. *Hydrological Processes*, 16(18), pp.3529-3542, <https://doi.org/10.1002/hyp.1236>, 2002.  
1155

1156 Kalnay, E., Kanamitsu, M., Kistler, R., Collins, W., Deaven, D., Gandin, L., Iredell, M., Saha, S., White, G., Woollen, J. and Zhu,  
1157 Y.: The NCEP/NCAR 40-year reanalysis project, *Bulletin of the American meteorological Society*, 77(3), pp.437-471,  
1158 [https://doi.org/10.1175/1520-0477\(1996\)077<0437:TNYRP>2.0.CO;2](https://doi.org/10.1175/1520-0477(1996)077<0437:TNYRP>2.0.CO;2), 1996.  
1159  
1160 Kalnay, E.: *Atmospheric modeling, data assimilation and predictability*. Cambridge university press, 2003.  
1161  
1162 Kapnick, S. and Hall, A.: Causes of recent changes in western North American snowpack. *Climate Dynamics*, 38(9-10), pp.1885-  
1163 1899, <https://doi.org/10.1007/s00382-011-1089-y>, 2012.  
1164  
1165 King, J.M., Cabrera, A.R. and Kelly, R.E.: The Snowtweets Project: Communicating snow depth measurements from specialists  
1166 and non-specialists via mobile communication technologies and social networks. AGU Fall Meeting Abstracts, Bibcode:  
1167 2009AGUFMED11A0562K, 2009.  
1168  
1169 Lader, R., Bhatt, U.S., Walsh, J.E., Rupp, T.S. and Bieniek, P.A.: Two-meter temperature and precipitation from atmospheric  
1170 reanalysis evaluated for Alaska, *Journal of Applied Meteorology and Climatology*, 55(4), pp.901-922,  
1171 <https://doi.org/10.1175/JAMC-D-15-0162.1>, 2016.  
1172  
1173 Lehning, M., Bartelt, P., Brown, B., Russi, T., Stöckli, U. and Zimmerli, M. SNOWPACK model calculations for avalanche  
1174 warning based upon a new network of weather and snow stations. *Cold Regions Science and Technology*, 30(1-3), pp.145-157,  
1175 [https://doi.org/10.1016/S0165-232X\(99\)00022-1](https://doi.org/10.1016/S0165-232X(99)00022-1), 1999.  
1176  
1177 Lehning, M., Völksch, I., Gustafsson, D., Nguyen, T.A., Stähli, M. and Zappa, MALPINE3D: a detailed model of mountain surface  
1178 processes and its application to snow hydrology. *Hydrological Processes: An International Journal*, 20(10), pp.2111-2128,  
1179 <https://doi.org/10.1002/hyp.6204>, 2006.  
1180  
1181 Li, D., Wigmore, O., Durand, M.T., Vander-Jagt, B., Margulis, S.A., Molotch, N.P. and Bales, R.C.: Potential of Balloon  
1182 Photogrammetry for Spatially Continuous Snow Depth Measurements. *IEEE Geoscience and Remote Sensing Letters*,  
1183 <https://doi.org/10.1109/LGRS.2019.2953481>, 2019.  
1184  
1185 Liston, G.E. and Elder, K.: A distributed snow-evolution modeling system (SnowModel), *Journal of Hydrometeorology*, 7(6),  
1186 pp.1259-1276, <https://doi.org/10.1175/JHM548.1>, 2006a.  
1187  
1188 Liston, G.E. and Elder, K.: A meteorological distribution system for high-resolution terrestrial modeling (MicroMet), *Journal of*  
1189 *Hydrometeorology*, 7(2), pp.217-234, <https://doi.org/10.1175/JHM486.1>, 2006b.  
1190  
1191 Liston, G.E., Haehnel, R.B., Sturm, M., Hiemstra, C.A., Berezovskaya, S. and Tabler, R.D.: Simulating complex snow distributions  
1192 in windy environments using SnowTran-3D. *Journal of Glaciology*, 53(181), pp.241-256,  
1193 <https://doi.org/10.3189/172756507782202865>, 2007.  
1194  
1195 Liston, G.E. and Hiemstra, C.A.: A simple data assimilation system for complex snow distributions (SnowAssim). *Journal of*  
1196 *Hydrometeorology*, 9(5), pp.989-1004, <https://doi.org/10.1175/2008JHM871.1>, 2008.  
1197

1198 Liston, G.E. and Hiemstra, C.A.: The changing cryosphere: Pan-Arctic snow trends (1979–2009). *Journal of Climate*, 24(21),  
1199 pp.5691-5712, <https://doi.org/10.1175/JCLI-D-11-00081.1>, 2011.  
1200

1201 López-Moreno, J.I., Fassnacht, S.R., Heath, J.T., Musselman, K.N., Revuelto, J., Latron, J., Morán-Tejeda, E. and Jonas, T.: Small  
1202 scale spatial variability of snow density and depth over complex alpine terrain: Implications for estimating snow water equivalent.  
1203 *Advances in water resources*, 55, pp.40-52, <https://doi.org/10.1016/j.advwatres.2012.08.010>, 2013.  
1204

1205 Lowry, C.S. and Fienen, M.N.: CrowdHydrology: crowdsourcing hydrologic data and engaging citizen scientists. *GroundWater*,  
1206 51(1), pp.151-156, <https://doi.org/10.1111/j.1745-6584.2012.00956.x>, 2013.  
1207

1208 Luce, C.H., Tarboton, D.G. and Cooley, K.R.: The influence of the spatial distribution of snow on basin-averaged snowmelt.  
1209 *Hydrological Processes*, 12(10-11), pp.1671-1683, [https://doi.org/10.1002/\(SICI\)1099-1085\(199808/09\)12:10/11<1671::AID-HYP688>3.0.CO;2-N](https://doi.org/10.1002/(SICI)1099-1085(199808/09)12:10/11<1671::AID-HYP688>3.0.CO;2-N), 1998.  
1210

1211

1212 Luojus, K., Pulliainen, J., Takala, M., Derksen, C., Rott, H., Nagler, T., Solberg, R., Wiesmann, A., Metsamaki, S., Malnes, E. and  
1213 Bojkov, B.: Investigating the feasibility of the GlobSnow snow water equivalent data for climate research purposes. In 2010 IEEE  
1214 International Geoscience and Remote Sensing Symposium (pp. 4851-4853), IEEE,  
1215 <https://doi.org/10.1109/IGARSS.2010.5741987>, 2010.  
1216

1217 Magnusson, J., Gustafsson, D., Hüsler, F. and Jonas, T.: Assimilation of point SWE data into a distributed snow cover model  
1218 comparing two contrasting methods. *Water resources research*, 50(10), pp.7816-7835, <https://doi.org/10.1002/2014WR015302>,  
1219 2014.  
1220

1221 Magnusson, J., Winstral, A., Stordal, A.S., Essery, R. and Jonas, T.: Improving physically based snow simulations by assimilating  
1222 snow depths using the particle filter. *Water Resources Research*, 53(2), pp.1125-1143, <https://doi.org/10.1002/2016WR019092>,  
1223 2017.  
1224

1225 Malik, M.J., van der Velde, R., Vekerdy, Z. and Su, Z. Assimilation of satellite-observed snow albedo in a land surface model.  
1226 *Journal of hydrometeorology*, 13(3), pp.1119-1130, <https://doi.org/10.1175/JHM-D-11-0125.1>, 2012.  
1227

1228 Mankin, J.S., Viviroli, D., Singh, D., Hoekstra, A.Y. and Diffenbaugh, N.S.: The potential for snow to supply human water demand  
1229 in the present and future. *Environmental Research Letters*, 10(11), p.114016, <https://doi.org/10.1088/1748-9326/10/11/114016>,  
1230 2015.  
1231

1232 Margulis, S.A., Giroto, M., Cortés, G. and Durand, M.: A particle batch smoother approach to snow water equivalent estimation.  
1233 *Journal of Hydrometeorology*, 16(4), pp.1752-1772, <https://doi.org/10.1175/JHM-D-14-0177.1>, 2015.  
1234

1235 Marks, D., Domingo, J., Susong, D., Link, T. and Garen, D.: A spatially distributed energy balance snowmelt model for application  
1236 in mountain basins, *Hydrological Processes*, 13(12-13), pp.1935-1959, [https://doi.org/10.1002/\(SICI\)1099-1085\(199909\)13:12/13<1935::AID-HYP868>3.0.CO;2-C](https://doi.org/10.1002/(SICI)1099-1085(199909)13:12/13<1935::AID-HYP868>3.0.CO;2-C), 1999.  
1237  
1238

1239 Massey Jr, F.J.:The Kolmogorov-Smirnov test for goodness of fit. *Journal of the American statistical Association*, 46(253), pp.68-  
1240 78, 1951.  
1241  
1242 McCreight, J.L., Small, E.E. and Larson, K.M.: Snow depth, density, and SWE estimates derived from GPS reflection data:  
1243 Validation in the western US. *Water Resources Research*, 50(8), pp.6892-6909, <https://doi.org/10.1002/2014WR015561>, 2014.  
1244  
1245 McGuire, M., Wood, A.W., Hamlet, A.F. and Lettenmaier, D.P.: Use of satellite data for streamflow and reservoir storage forecasts  
1246 in the Snake River Basin. *Journal of Water Resources Planning and Management*, 132(2), pp.97-110,  
1247 [https://doi.org/10.1061/\(ASCE\)0733-9496\(2006\)132:2\(97\)2006](https://doi.org/10.1061/(ASCE)0733-9496(2006)132:2(97)2006).  
1248  
1249 McLaughlin, D.: An integrated approach to hydrologic data assimilation: interpolation, smoothing, and filtering. *Advances in*  
1250 *Water Resources*, 25(8), pp.1275-1286, [https://doi.org/10.1016/S0309-1708\(02\)00055-6](https://doi.org/10.1016/S0309-1708(02)00055-6), 2002.  
1251  
1252 McKinley, D.C., Miller-Rushing, A.J., Ballard, H.L., Bonney, R., Brown, H., Cook-Patton, S.C., Evans, D.M., French, R.A.,  
1253 Parrish, J.K., Phillips, T.B. and Ryan, S.F.: Citizen science can improve conservation science, natural resource management, and  
1254 environmental protection. *Biological Conservation*, 208, pp.15-28, <https://doi.org/10.1016/j.biocon.2016.05.015>, 2017.  
1255  
1256 McMillan, H.K., Hreinsson, E.Ö., Clark, M.P., Singh, S.K., Zammit, C. and Uddstrom, M.J.: Operational hydrological data  
1257 assimilation with the recursive ensemble Kalman filter. *Hydrology and Earth System Sciences*, 17(1), pp.21-38,  
1258 <https://doi.org/10.5194/hess-17-21-2013>, 2013.  
1259  
1260 Mernild, S.H., Liston, G.E., Hasholt, B. and Knudsen, N.T.: Snow distribution and melt modeling for Mittivakkat Glacier,  
1261 Ammassalik Island, southeast Greenland. *Journal of Hydrometeorology*, 7(4), pp.808-824, <https://doi.org/10.1175/JHM522.1>,  
1262 2006.  
1263  
1264 Mernild, S.H., Liston, G.E., Hiemstra, C.A., Malmros, J.K., Yde, J.C. and McPhee, J.: The Andes Cordillera. Part I: snow  
1265 distribution, properties, and trends (1979–2014), *International Journal of Climatology*, 37(4), pp.1680-1698,  
1266 <https://doi.org/10.1002/joc.4804>, 2017a.  
1267  
1268 Mernild, S.H., Liston, G.E., Hiemstra, C.A., Yde, J.C., McPhee, J. and Malmros, J.K.: The Andes Cordillera. Part II: Rio Olivares  
1269 Basin snow conditions (1979–2014), central Chile, *International Journal of Climatology*, 37(4), pp.1699-1715,  
1270 <https://doi.org/10.1002/joc.4828>, 2017b.  
1271  
1272 Mesinger, F., DiMego, G., Kalnay, E., Mitchell, K., Shafran, P.C., Ebisuzaki, W., Jović, D., Woollen, J., Rogers, E., Berbery, E.H.  
1273 and Ek, M.B.: North American regional reanalysis, *Bulletin of the American Meteorological Society*, 87(3), pp.343-360,  
1274 <https://doi.org/10.1175/BAMS-87-3-343>, 2006.  
1275  
1276 Molotch, N.P. and Bales, R.C.: Scaling snow observations from the point to the grid element: Implications for observation network  
1277 design. *Water Resources Research*, 41(11), <https://doi.org/10.1029/2005WR004229>, 2005a.  
1278

1279 Molotch, N.P., Colee, M.T., Bales, R.C. and Dozier, J.: Estimating the spatial distribution of snow water equivalent in an alpine  
1280 basin using binary regression tree models: the impact of digital elevation data and independent variable selection. *Hydrological*  
1281 *Processes: An International Journal*, 19(7), pp.1459-1479, <https://doi.org/10.1002/hyp.5586>, 2005b.

1282

1283 Mote, P.W., Li, S., Lettenmaier, D.P., Xiao, M. and Engel, R.: Dramatic declines in snowpack in the western US. *Npj Climate and*  
1284 *Atmospheric Science*, 1(1), pp.1-6, <https://doi.org/10.1038/s41612-018-0012-1>, 2018.

1285

1286 NOHRSC: Snow Data Assimilation System (SNODAS) Data Products at NSIDC, Version 1. Boulder, Colorado USA. NSIDC:  
1287 National Snow and Ice Data Center. doi: <https://doi.org/10.7265/N5TB14TC>, 2004.

1288

1289 Pagano, T., Garen, D., Perkins, T., and Pasteris, P.: Daily updating of operational statistical seasonal water supply forecasts for the  
1290 western U.S., *J. Am. Water Resour. As.*, 45, 767–778, <https://doi.org/10.1111/j.1752-1688.2009.00321.x>, 2009.

1291

1292 Painter, T.H., Berisford, D.F., Boardman, J.W., Bormann, K.J., Deems, J.S., Gehrke, F., Hedrick, A., Joyce, M., Laidlaw, R.,  
1293 Marks, D. and Mattmann, C.: The Airborne Snow Observatory: Fusion of scanning lidar, imaging spectrometer, and physically-  
1294 based modeling for mapping snow water equivalent and snow albedo. *Remote Sensing of Environment*, 184, pp.139-152,  
1295 <https://doi.org/10.1016/j.rse.2016.06.018>, 2016.

1296

1297 Park, S.K. and Xu, L. eds.: Data assimilation for atmospheric, oceanic and hydrologic applications (Vol. 2). Springer Science &  
1298 Business Media, 2013.

1299

1300 Pistocchi, A.: Simple estimation of snow density in an Alpine region. *Journal of Hydrology: Regional Studies*, 6, pp.82-89,  
1301 <https://doi.org/10.1016/j.ejrh.2016.03.004>, 2016.

1302

1303 Pomeroy, J.W., Gray, D.M. and Landine, P.G. The prairie blowing snow model: characteristics, validation, operation. *Journal of*  
1304 *Hydrology*, 144(1-4), pp.165-192, [https://doi.org/10.1016/0022-1694\(93\)90171-5](https://doi.org/10.1016/0022-1694(93)90171-5), 1993.

1305

1306 Rabier, F.: Overview of global data assimilation developments in numerical weather-prediction centres. *Quarterly Journal of the*  
1307 *Royal Meteorological Society: A journal of the atmospheric sciences, applied meteorology and physical oceanography*, 131(613),  
1308 pp.3215-3233, <https://doi.org/10.1256/qj.05.129>, 2005.

1309

1310 Reges, H.W., Doesken, N., Turner, J., Newman, N., Bergantino, A. and Schwalbe, Z.: COCORAHs: The evolution and  
1311 accomplishments of a volunteer rain gauge network. *Bulletin of the American Meteorological Society*, 97(10), pp.1831-1846,  
1312 <https://doi.org/10.1175/BAMS-D-14-00213.1>, 2016.

1313

1314 Reichle, R.H., McLaughlin, D.B. and Entekhabi, D.: Hydrologic data assimilation with the ensemble Kalman filter. *Monthly*  
1315 *Weather Review*, 130(1), pp.103-114, [https://doi.org/10.1175/1520-0493\(2002\)130<0103:HDAWTE>2.0.CO;2](https://doi.org/10.1175/1520-0493(2002)130<0103:HDAWTE>2.0.CO;2), 2002.

1316

1317 Reichle, R.H.: Data assimilation methods in the Earth sciences. *Advances in water resources*, 31(11), pp.1411-1418,  
1318 <https://doi.org/10.1016/j.advwatres.2008.01.001/>, 2008.

1319



1320 Rice, R. and Bales, R.C.: Embedded-sensor network design for snow cover measurements around snow pillow and snow course  
1321 sites in the Sierra Nevada of California. *Water Resources Research*, 46(3), <https://doi.org/10.1029/2008WR007318>, 2010.  
1322

1323 Riemann, R., Wilson, B.T., Lister, A. and Parks, S.: An effective assessment protocol for continuous geospatial datasets of forest  
1324 characteristics using USFS Forest Inventory and Analysis (FIA) data. *Remote Sensing of Environment*, 114(10), pp.2337-2352,  
1325 <https://doi.org/10.1016/j.rse.2010.05.010>, 2010.  
1326

1327 Rivington, M., Matthews, K.B., Bellocchi, G. and Buchan, K.: Evaluating uncertainty introduced to process-based simulation  
1328 model estimates by alternative sources of meteorological data. *Agricultural Systems*, 88(2-3), pp.451-471,  
1329 <https://doi.org/10.1016/j.agsy.2005.07.004>, 2006.  
1330

1331 Saha, S., Moorthi, S., Pan, H.L., Wu, X., Wang, J., Nadiga, S., Tripp, P., Kistler, R., Woollen, J., Behringer, D. and Liu, H.: The  
1332 NCEP climate forecast system reanalysis. *Bulletin of the American Meteorological Society*, 91(8), pp.1015-1058,  
1333 <https://doi.org/10.1175/2010BAMS3001.1>, 2010.  
1334

1335 Saha, S., Moorthi, S., Wu, X., Wang, J., Nadiga, S., Tripp, P., Behringer, D., Hou, Y.T., Chuang, H.Y., Iredell, M. and Ek, M.:  
1336 The NCEP climate forecast system version 2. *Journal of Climate*, 27(6), pp.2185-2208, <https://doi.org/10.1175/JCLI-D-12-00823.1>, 2014.  
1337

1338 Schmucki, E., Marty, C., Fierz, C. and Lehning, M.: Evaluation of modelled snow depth and snow water equivalent at three  
1339 contrasting sites in Switzerland using SNOWPACK simulations driven by different meteorological data input. *Cold Regions  
1340 Science and Technology*, 99, pp.27-37, <https://doi.org/10.1016/j.coldregions.2013.12.004>, 2014.  
1342

1343 Schaefer, M. and Woodyer, T.: Assessing absolute and relative accuracy of recreation-grade and mobile phone GNSS devices: a  
1344 method for informing device choice. *Area*, 47(2), pp.185-196, <https://doi.org/10.1111/area.12172>, 2015.  
1345

1346 Schlögl, S., Marty, C., Bavay, M. and Lehning, M.: Sensitivity of Alpine3D modeled snow cover to modifications in DEM  
1347 resolution, station coverage and meteorological input quantities. *Environmental modelling & software*, 83, pp.387-396,  
1348 <https://doi.org/10.1016/j.envsoft.2016.02.017>, 2016.  
1349

1350 Schneider, C., Laizé, C.L.R., Acreman, M.C. and Flörke, M.: How will climate change modify river flow regimes in Europe?.  
1351 *Hydrology and Earth System Sciences*, 17(1), pp.325-339, <https://doi.org/10.5194/hess-17-325-2013>, 2013.  
1352

1353 Seibert, J., Strobl, B., Etter, S., Hummer, P. and van Meerveld, H.J.: Virtual staff gauges for crowd-based stream level observations.  
1354 *Frontiers in Earth Science - Hydrosphere*, 7, p.70, <https://doi.org/10.3389/feart.2019.00070>, 2019.  
1355

1356 Serreze, M.C., Clark, M.P., Armstrong, R.L., McGinnis, D.A. and Pulwarty, R.S.: Characteristics of the western United States  
1357 snowpack from snowpack telemetry (SNOTEL) data. *Water Resources Research*, 35(7), pp.2145-2160,  
1358 <https://doi.org/10.1029/1999WR900090>, 1999.  
1359

1360 Shulski, M. and Wendler, G.: *The climate of Alaska*. University of Alaska Press, 2007.  
1361

1362 Silvertown, J.: A new dawn for citizen science. *Trends in ecology & evolution*, 24(9), pp.467-471,  
1363 <https://doi.org/10.1016/j.tree.2009.03.017>, 2009.

1364

1365 Sturm, M., Holmgren, J. and Liston, G.E.: A seasonal snow cover classification system for local to global applications. *Journal of*  
1366 *Climate*, 8(5), pp.1261-1283, [https://doi.org/10.1175/1520-0442\(1995\)008<1261:ASSCCS>2.0.CO;2](https://doi.org/10.1175/1520-0442(1995)008<1261:ASSCCS>2.0.CO;2), 1995.

1367

1368 Sturm, M., Taras B., Liston G., Derksen, C., Jonas T., and Lea, J.: Estimating Snow Water Equivalent Using Snow Depth Data  
1369 and Climate Classes. *Journal of Hydrometeorology* 11 (6): 1380–94. <https://doi.org/10.1175/2010JHM1202.1>, 2010a.

1370

1371 Sturm, M. and Wagner, A.M.: Using repeated patterns in snow distribution modeling: An Arctic example. *Water Resources*  
1372 *Research*, 46(12), <https://doi.org/10.1029/2010WR009434>, 2010b.

1373

1374 Sturm, M.: White water: Fifty years of snow research in WRR and the outlook for the future. *Water Resources Research*, 51(7),  
1375 pp.4948-4965, <https://doi.org/10.1002/2015WR017242>, 2015.

1376

1377 Trujillo, E., Molotch, N.P., Goulden, M.L., Kelly, A.E. and Bales, R.C.: Elevation-dependent influence of snow accumulation on  
1378 forest greening. *Nature Geoscience*, 5(10), pp.705-709, <https://doi.org/10.1038/ngeo1571>, 2012.

1379

1380 van Meerveld, H. J. I., Vis, M. J. P., and Seibert, J.: Information content of stream level class data for hydrological model  
1381 calibration, *Hydrol. Earth Syst. Sci.*, 21, 4895-4905, <https://doi.org/10.5194/hess-21-4895-2017>, 2017.

1382

1383 Viviroli, D., Dürr, H.H., Messerli, B., Meybeck, M. and Weingartner, R.: Mountains of the world, water towers for humanity:  
1384 Typology, mapping, and global significance. *Water resources research*, 43(7), <https://doi.org/10.1029/2006WR005653>, 2007.

1385

1386 Wagner, W.: Investigating the snow climate of Turnagain Pass, Alaska. In *Proceedings of the International Snow Science*  
1387 *Workshop*, Anchorage, AK (pp. 913-917), 2012.

1388

1389 Wiggins, A. and Crowston, K.: From conservation to crowdsourcing: A typology of citizen science. In 2011 44th Hawaii  
1390 international conference on system sciences (pp. 1-10). IEEE, <https://doi.org/10.1109/HICSS.2011.207>, 2011.

1391

1392 Wrzesien, M.L., Durand, M.T., Pavelsky, T.M., Howat, I.M., Margulis, S.A. and Huning, L.S.: Comparison of methods to estimate  
1393 snow water equivalent at the mountain range scale: a case study of the California Sierra Nevada. *Journal of Hydrometeorology*,  
1394 18(4), pp.1101-1119, <https://doi.org/10.1175/JHM-D-16-0246.1>, 2017.

1395

1396 Yeeles, A.: Citizen snow-scientists trek into the back country. *Nature Climate Change*, 8(11), p.944,  
1397 <https://doi.org/10.1038/s41558-018-0329-0>, 2018.

1398

1399 [Young, J.C., Pettit, E., Arendt, A., Hood, E., Liston, G.E. and Beamer, J.: A changing hydrological regime: Trends in magnitude](#)  
1400 [and timing of glacier ice melt and glacier runoff in a high latitude coastal watershed. \*Water Resources Research\*,](#)  
1401 [p.e2020WR027404, 2020.](#)